U.PORTO

FEUP FACULDADE DE ENGENHARIA
UNIVERSIDADE DO PORTO

Strength and fracture energy of adhesives for the automotive industry

AUTHOR:

CARLOS M. S. CANTO - 080504114

SUPERVISOR:

PROFESSOR LUCAS F. M. DA SILVA

Departamento de Engenharia Mecânica

FACULDADE DE ENGENHARIA DA UNIVERSIDADE DO PORTO

Oporto, Portugal, July of 2013

REPORT DEVELOPED AS A RESULT OF THE WORK DONE FOR THE MASTER THESIS IN MECHANICAL ENGINEERING.

Strength and fracture energy of adhesives for the automotive industry

AUTHOR:

CARLOS M. S. CANTO - 080504114

SUPERVISOR:

PROFESSOR LUCAS F. M. DA SILVA

Departamento de Engenharia Mecânica

FACULDADE DE ENGENHARIA DA UNIVERSIDADE DO PORTO

Oporto, Portugal, July of 2013

The present dissertation presents the work done for the acquisition of the master degree in mechanical engineering. It has been developed in conjunction with laboratory of adhesive and laboratory of technological trials from the department of mechanical engineering of FEUP.

Carlos Maurício Sousa Canto

FACULDADE DE ENGENHARIA DA UNIVERSIDADE DO PORTO

Departamento de Engenharia Mecânica

Rua Dr. Roberto Frias

4200 – 465 Porto

Portugal

em08114@fe.up.pt

“It is not in the stars to hold our destiny but in ourselves.”

William Shakespeare

Abstract

Adhesives used in automotive industry must be cheap and have good mechanical properties when bonding metal parts or composites and although there are disadvantages some adhesive bonds are stronger than the materials being bonded together. In some cases it may be the only solution to efficiently bond two surfaces together (ex: carbon fibber and all composites in general) and could be the solution for building lighter and more efficient cars. Nowadays, design is initiated using computer aided simulation and in order to predict the mechanical behaviour of adhesives bonds with a finite element analysis (FEA) a full characterization of the adhesive is necessary.

In this study two different adhesives were characterized: a high elongation and high toughness epoxy adhesive, and a toughened epoxy adhesive. Failure strength tests were conducted using both structural adhesives. Tensile bulk tests were performed using long dogbone specimens to characterize the adhesives at room temperature. In addition, a study of size dependence of the bulk specimen was also carried out.

Secondly, numerical models of double cantilever beam (DCB) specimens using cohesive zone models were developed using Abaqus®. This was used to develop an optimized smaller DCB specimen that allows a reliable characterization of adhesive fracture toughness. Afterwards fracture strength tests were used to characterize a toughened epoxy adhesive loaded in mode I and validate the numerical results.

Lastly, a drop weight impact test was conducted to characterize the mechanical behaviour of a high elongation and high ductility adhesive with low yield strength steel adherends.

Resumo

Os adesivos usados na indústria automóvel têm de ser economicamente competitivos e ter boas propriedades mecânicas quando ligam metais ou compósitos. As ligações adesivas são por vezes tão eficientes que acabam por ser mais resistentes que os substratos a ligar. Em outros casos, as ligações adesivas são mesmo a única forma eficaz de fazer ligações, (e.g. fibra de carbono e os compósitos em geral) e podem ser a solução para construir carros mais leves. Hoje em dia o design é auxiliado por ferramentas numéricas de simulação, ajudando a prever o comportamento das juntas adesivas. Para tal é preciso caracterizar o adesivo a usar no modelo de elementos finitos.

Nesta tese foi feita a caracterização de dois adesivos diferentes. O primeiro, com grande elongação e grande tenacidade e o segundo, um epóxido estrutural. A caracterização á tracção foi feita com provetes maciços longos de adesivos num estado unidireccional de tensão. Também foi feito um estudo de factores de escala nos provetes sendo para tal construídos provetes de pequenas dimensões. Todos os provetes foram testados à temperatura ambiente.

Numa segunda etapa, foi usado o modelo coesivo do Abaqus® para fazer um estudo numérico dos provetes DCB. O objectivo foi desenvolver um provete DCB de reduzidas dimensões que permitisse uma caracterização fiel da tenacidade em modo I do adesivo. Em seguida, foram realizados ensaios experimentais para caracterizar os adesivos e validar os resultados numéricos obtidos.

Por fim, foi feito um ensaio de impacto para caracterizar a resposta do adesivo com grande elongação e avaliar se seria uma boa solução a usar nas chapas dos automóveis utilitários.

Acknowledgements

I would like to thank Professor Lucas da Silva for the guidance and advice both important for the completion of this thesis. Furthermore, I am very grateful to him for giving me the opportunity to work under his supervision.

I want also to acknowledge Professor Raul Campilho and Doctor Mariana Banea for the many hours that we spent discussing some of the results, the advice and experience shared.

When doing the experimental work Engineer Ricardo Carbas was always available both as a teacher and a friend and my gratitude goes to him.

All the personnel in the Adhesives group of FEUP, specially Marcelo, for the help and company in the long hours spent studying adhesives and developing this thesis.

The company NAGASE CHEMTEX® (Osaka, Japan) for the information provided, supplying of the epoxy adhesive XNR6852 and sponsoring the present work.

Also I would like to acknowledge the mechanical workshop of FEUP for helping in the production of the specimens.

And lastly, all my family and friends for the support and care that were of the most importance to persevere and accomplish this final step in my master degree.

Contents

List of publications

1. D. F. S. Saldanha, C. Canto, L. F. M. da Silva, R. J. C. Carbas, F. J. P. Chaves, K. Nomura, T.Ueda, Mechanical characterization of a high elongation and high toughness epoxy adhesive, International Journal of Adhesion and Adhesives, accepted for publication.

List of tables

List of figures

List of acronyms

CT	Compact tension
DCB	Double cantilever beam
DMA	Dynamic mechanical analysis
ENF	End notched flexure
EVA	Ethylene-vinyl acetate
FEA	Finite element analysis
FPZ	Fracture process zone
PU	Polyurethane
SENB	Single-edge notched bending
SLJ	Single lap joint
CCM	Compliance calibration method
CBT	Compliance beam theory
CBBM	Compliance-Based beam method

List of symbols

δ	Displacement
ε	Strain
η	Dumping constant
σ	Normal stress
τ	Shear stress
a	Crack length
a_0	Initial crack length
a_{eq}	Equivalent Crack length
b	Substrate width
C	Compliance
E	Young´s modulus
E_f	Corrected flexure modulus
G	Shear modulus
G_I	Fracture toughness in mode I
G_{IC}	Critical fracture toughness in mode I
G_{II}	Fracture toughness in mode II
G_{IIC}	Critical fracture toughness in mode II
h	Substrate thickness
k	Rigidity
K_I	Stress intensity factor
K_{IC}	Critical stress intensity factor
l	Overlap length
m	Geometric factor
P	Applied load
Tg	Glass transition temperature
Y	Correction coefficient
Δ	Correction for the crack tip rotation
v	Poisson´s ratio

1. Introduction

1.1 Background and motivation

Adhesive bonding is increasingly being used in structural applications such as in rail vehicle or automotive industry. However, design in terms of durability still needs a lot of research. It is at the moment difficult to predict the failure load after exposure to load under static or dynamic conditions, temperature and humidity over a long period of time. With the rapid increase in numerical computing power there have been attempts to formalize the different environmental contributions in order to provide a procedure to predict assembly durability, based on an initial identification of diffusion coefficients and mechanical parameters.

Adhesive joints can be designed with the help of analytical method or numerical tools. For complex predictions that include various factors such as the effect of temperature and humidity, only the numerical methods can be used.

1.2 Problem definition

Cohesive zone elements have been developed to simulate the static damage but also damage due to fatigue and more recently due to the environment. However, the adhesive behaviour also depends on temperature and strain rate. For a complete modelling, the cohesive element should also include these effects.

1.3 Objectives

The objective of this thesis was to lay the foundations for a project to develop a cohesive element that includes the effect of temperature, humidity, time (viscoelastic behaviour of the adhesive) and fatigue. In order to accomplish it a complete mechanical characterization of the adhesives used has to be done and optimization of the resources studied.

1.4 Research methodology

In order to achieve the aim of this thesis, the following work was done:

- An overview of some advantages and good practices was done. This was followed by a study of the most used adhesives and their common characteristics in order to grasp the huge variety of structural adhesives available.
- Failure strength tests were carried out using bulk specimens to determine the tensile adhesive properties. Also, small dogbone specimens were produced to validate the geometry to be used in the durability project.
- Numerical simulations using cohesive zone models, in which the failure behaviour is expressed by a bilinear traction separation law, were developed using Abaqus®. This was done to find an optimum small specimen that would enable a quicker aging process.
- DCB tests were done to characterize the fracture toughness of a toughened epoxy adhesive and validate the results of the numerical simulation.
- Impact test is an important feature when designing an adhesive joint for the automotive industry. From previous studies it was concluded that adhesive joints behaviour is changes at high strain rates so to investigate it a drop weight impact test was conducted.

1.5 Outline of thesis

The second chapter of this thesis consists of a literature review on adhesives. Some general properties were compiled as well as an overview of the most used adhesives.

The third chapter is a summary of the Failure strength tests conducted using two structural epoxy adhesives, XNR 6852 , supplied by NAGASE CHEMTEX® (Osaka, Japan), and SikaPower 4720, supplied by SIKA® (Portugal, Vila Nova de Gaia). Tensile bulk tests were performed using long dogbone to characterize the adhesive and compare with other available solution. In addition a study of size dependence of the bulk specimen was also carried out.

The forth chapter begins with a numerical study of the double cantilever beam (DCB) test. This was done to develop an optimized smaller DCB specimen that would allow a reliable characterization of adhesive fracture toughness. This was done using Abaqus®´s cohesive zone models. Afterwards fracture strength tests, DCB tests, were used to characterize an adhesive bond solicited in mode I and validate the numerical findings. In

this case toughened epoxy SikaPower 4720 was used and its fracture toughness studied as a function of geometry.

Lastly, in the fifth chapter an impact test was conducted to characterize the mechanical behaviour of the high elongation and high ductility adhesive XNR6852, with low yield strength steel adherends.

2. Literature review

An adhesive is defined as a substance that binds two surfaces together and resists separation. Usually there are many terms to refer to it, some common ones are: glue, cement, mucilage, mastic or paste.

In order to understand adhesives and adhesion there can be two different approaches. A practical approach, concerned with the mechanical properties resulting from the adhesion, and a theoretical approach, evaluating the reasons behind the molecular bonding of the surfaces. As a result, to accurately understand and predict the adhesives joint properties different areas are investigated such as: physics, chemistry and mechanics. This thesis focuses on the mechanical properties.

The use of adhesive bonded joints has increased in recent years. The reason is the many advantages that a well-constructed adhesive joint bring to the structural integrity when compared to the traditional mechanical fasteners. Some of the advantages are:

a) a more uniform stress distribution,
b) it enables the design of better looking shapes as a consequence of the inexistence of holes from the bolts or rivets and the marks from welding (Figure 1),
c) in many mechanical applications vibration damping is also interesting when compared with the traditional joining methods,
d) joining two materials with different expansion coefficient can be done with more efficiency due to the deformation of the adhesive,
e) it provides very efficient joining of steel sheets,
f) design is more versatile since adhesives can join different materials and concepts,
g) ease of fabrication and the possibility to be automated, saving money and time,
h) it may have a sealing role. [1-3]

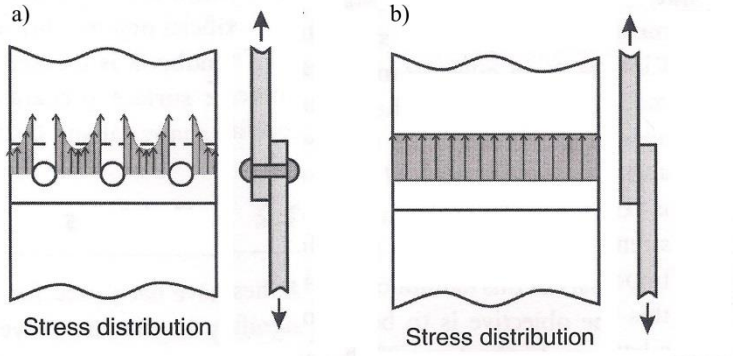

Figure 1 - Comparison of two stress distribution caused by tension on a sheet part, a) traditional riveted assembly and stress distribution, b) stress distribution on adhesive bonded sheets. [1]

On the other hand, some disadvantages are:

a) the service temperature is limited,
b) requires in most cases a surface preparation,
c) due to a huge variety of adhesives available selecting a suitable one requires some experience,
d) adhesive bonding is weak when loaded in tension. The two main cases to be avoided are cleavage and peel stresses,
e) avoiding localized stresses on the adhesive is not always possible and can cause rupture of the adhesive,
f) in consequence of its polymeric nature heat and humidity are very harmful,
g) the joint cannot be built instantly and usually needs a holding mechanism,
h) needs curing at high temperatures in most cases,
i) although there has been improvements in the quality control of adhesive joints it is still a very hard task to accomplish.[1-3]

The adhesives industry is very diverse with multiple applications in areas such as: aeronautical, aerospace, automotive, shoe, furniture and others. With many applications and a market share already well-established the future for adhesives looks promising. According to a study from Ceresana®, 2012, on adhesive markets, it is concluded that it is expanding with growth rates of about 2.9% for the next 8 years. This evolution is predicted as a result of the rapid increase in the demand of consumer goods in the Asia-Pacific region.

2.1 Adhesive properties

Adhesives are polymeric by nature and are formed by large molecules, polymers, with small groups of atoms, monomers. The diversity of viable combinations for monomers is great and, as a consequence, the number of polymeric compounds that result are vast. On top of it, there are also mixed adhesives, resulting from a combination of several polymeric compounds. As a consequence the classification of adhesive is accomplished in different ways. Among the most common are:

a) Polymer base; natural or synthetic.
b) Chemical composition; thermoplastic, thermoset or rubber.
c) Physical forms; one or multiple components, films, tape, powder.

d) Chemical families; epoxy, polyamides and others.

e) Function; structural or non-structural. [1, 4]

2.1.1 General properties

In this thesis there is a particular interest in structural adhesives and their mechanical properties. A structural adhesive is an adhesive that transfer loads between adherends and usually have a shear strength higher than 5 MPa. Typically, structural adhesives are cross-linked/thermosetting polymers even though some thermoplastics are used. [7]

The strength of properly made adhesive joints is directly related to the strength of the adhesive. It has also been proved that failure is unlikely to occur at the interface and only in cases of poor surface preparation it is likely to take place. [5] Furthermore, since in most cases the adherends (ex. metals and carbon fibber) have a higher rigidity than the adhesive, the displacement will be mainly due to strain in the adhesive. Some common strength properties are presented in Table 1.

Table 1 – Comparative values of stiffness and strength of common structural materials.*

	Material	Relative density	Young´s modulus (GPa)	Shear modulus (GPa)	Tensile strength (MPa)
Common Structural materials	Mild steel	7.5	210	80	450
	Aluminium	2.6	70	26	550
	Carbon fiber reinforced composite, quasi-isotropic	1.55	110	45	800
	Wood (along grain)	0.7	13	1	80
Common Adhesives	Epoxy adhesive	1.25	3	1.2	60
	Polyurethanes	1.1	0.02	0.008	40
	Phenolics	1.3	3.5	1.4	50

*Information compiled from several text books and databases, illustrative only.

The choice of the adhesive for a particular application is not unique. Usually there are a variety of adhesives suitable and surface pre-treatments that can be applied to improve the joint performance. Also, the surface type can condition the adhesive selection for the task. For example, in the case of thermoplastic substrates, some adhesives may have a detrimental effect producing effects such as crazing, swelling, dissolutions or may be simply incompatible. On the other hand, some adhesives such as epoxies are versatile and will bond to different substrates.[6]

When selecting adhesives, some key factors to consider in the fabrication process are: joint performance (load, operating environment, durability), substrates type, adhesive form, costs, aesthetics, manufacturing process, application, health requirements and pre-treatments. Finally testing and validation is recommended to ensure the process quality.[1]

Since the diversity of adhesives available is extensive, an accurate choice is hard and will require experience. An overview of the most used structural adhesives is presented in Table 2 with a compilation of several general properties.

2.1.2 Temperature related properties

a) Glass transition temperature

The glass transition temperature, T_g, is the most important temperature in polymers and is a property of the amorphous part. It marks a transition from a glass-like structure to a rubber-like state. It is not a phase transition but a change in the derivative of the fundamental quantities with respect to temperature.

Although in some polymer (linear and very regular) the transition is masked, this is not the case for amorphous polymers where above T_g the long coiled molecular chains can rearrange and extend. This behaviour is mostly unwanted in rigid structures because the viscoelastic nature of the polymer will result in fast stress relaxation, low modulus and strength. In conclusion, the structural adhesives are expected to work below their T_g.[1, 5]

b) Decomposition temperature

Using adhesives above this temperature will completely destroy the joint and only for a short time there will be relevant mechanical properties. This is important for military projectiles for it relies on the char strength for a short period of time.[5]

c) Melting temperature

Opposed to the glass transition the melting temperature is not very important for adhesives because crystalline melting does not take place in amorphous polymers. Although of little importance, some adhesives do exhibit cristallinity such as: ethylene-vinyl acetate (EVA) and polyamides hot melts; polyvinylalcohol, polychloroprene and starch. [1]

Table 2 – General properties of the most common structural adhesives. **

Type	Material	Subtype	Service temperature (ºC)		Advantages	Disadvantages	Environment resistance			Cure	Applications	Cost*	Substrate material
			Minimum	Maximum			Water	Solvent	Oil				
Rigid adhesives	Epoxy	Two part epoxy	-40	100	Strength, durability	Slow curing, occasional voids	Good	Good	Good	Room temperature (accelerated cure with high temperature)	Aircraft, helicopters, cars, trains, sports equipment, etc.	Cheap/ Moderate	Metals, Ceramics, Wood, rigid PVC, rigid PE, rigid PP, PC and Teflon
		One part epoxy	-40	180	Strength and durability	Storage, Cures at high temperature	Excellent	Excellent	Excellent	High temperature (around 150ºC)	Aircraft, helicopters, cars, trains, sports equipment, etc.	Cheap/ Moderate	
	Acrylics	Anaerobics	-55	150	Little surface preparation	Thin bondline	Good	Depends on formulation	Good	Cure through a free radical mechanism (absence of oxygen).	Toys, Medical industry	Expensive	Metals and Ceramics
		Cyanoacrylates	-30	80	Fast cure	Can´t bond large areas, Brittle, Bad gap filling	Weak	Fair/Good	Good	Cures in seconds/minutes at room temperature	Jewellery, Electronic components, Toys, Sports equipment	Expensive	Metals, Ceramics, Cellulose acetate
		Modified	-40	120	Fast cure, Can bond unprepared surfaces, Good environment resistance	Lower strength and stiffness than epoxies.	Good	Good	Good	Catalysed reaction by an initiator	Automotive applications, Metallic furniture	Expensive	Metals, Ceramics, Wood, rigid PVC, PC
	Phenolics	Nitrile-phenolics	-40	160	Fire resistant	Difficult processing, Brittle, Porous bondline	Excellent	Good	Good	Moderate temperature and high pressure	Wood industry, Metals	Cheap/ Moderate	Metals, Paper, Leather, rigid PE, rigid PP
		Polyvinyl-phenolics											Metals
		Neoprene-phenolics											Metals, Leather
	Polyaromatics	Polyimides, Bismaleimide	-40	280	Strength at high temperature	Difficult processing, Brittle (20ºC), Porous bondline	Excellent	Excellent	Excellent	High temperature and high pressure	Semiconductor industry, high temperature applications	Moderate	Metals
Flexible adhesives	Polyurethanes	-	-200	120	Good strength at low temperatures, Toughness, Wetting ability	Moisture cure, limited temperature resistance	Fair	Fair/Good	Fair/Good	Room temperature	Cryogenic applications, Automotive industry, Shoe industry	Moderate	Metals, Ceramics, Wood, Polyurethane, PVC, Cellulose acetate, PC
	Silicones	-	-100	300	Temperature range, Chemical stability, Electrical properties	Poor strength, Cost	Excellent	Good	Excellent	Room temperature	Electrical insulation, Glass assembly, Food processing equipment	Moderate/ Expensive	Metals, Glass

*price ranges from 1 to 40 euro/kg

**Information compiled from several text books and databases, illustrative only.

d) Thermal expansion

The thermal expansion coefficient of the adhesive is much higher than that of typical metallic substrates, which can lead to damaging interfacial stresses. The expansion can be reduced by the addition of mineral fillers.[1]

2.1.3 Viscoelasticity

In the elastic domain of metals an imposed stress will generate an extension proportional to it. However, in polymers the tensile behaviour is strongly influenced by time and the instantaneous response will be a small fraction of the total deformation.

Figure 2 shows two different models to describe viscoelasticity. The Maxwell model (Figure 2 - a) is described by:

$$\frac{d\varepsilon}{dt} = \frac{1}{\eta}S + \frac{1}{k}\frac{d\sigma}{dt} \quad (1)$$

In Equation 1, σ represents stress, ε the strain, η and k are constants relating to the dashpot viscosity and the rigidity of the spring respectively. According to Equation 1 if the deformation is constant ($d\varepsilon/dt = 0$) the stress will decay to zero, commonly known as stress relaxation.

The Voigt model (Figure 2 - b) is described by:

$$\sigma = \eta\frac{d\varepsilon}{dt} + k\varepsilon \quad (2)$$

In this model the deformation and its recovery is subjected to a time dependency, and this constant is commonly known as retardation time.

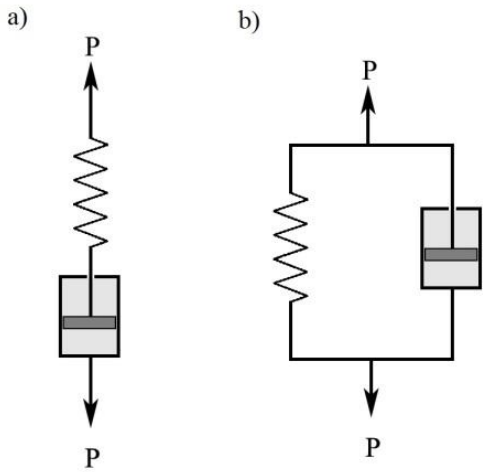

Figure 2 - Schematic models of viscoelastic behaviour, a) Maxwell model, b) Voigt model.

If the stress is applied during a period of time much smaller than the relaxation and retardation times the behaviour is determined by the spring. Typically, for polymers below the glass transition temperature, the relaxation time is infinitely long making the response elastic but time dependent. If the temperature is raised, the viscous component becomes increasingly important, especially above the T_g.[1, 5-7]

2.2 Analysis of adhesive joints

For complex geometries, a finite element analysis (FEA) is preferable however, for a fast and easy answer a closed-form analysis is usually used.[1, 3, 8]

2.2.1 Analytical approach

In the literature, most attention is given to single lap joint (SLJ) specimens for it is an efficient geometry to characterize an adhesive joint. For this geometry, generally, failure takes place in the adhesive and the stress distribution in that region was subjected to extensive study from many researchers.

For the analysis, some simplifying assumptions are made: substrates deformation due to tension and bending only and adhesive stresses restricted to peel and shear are assumed to be constant across the adhesive layer. However, the stresses in the adhesive are not uniform because of differential straining and the eccentricity of the loading path.[2, 8, 9]

a) Linear elastic analysis

A common and simple analysis is to consider undeformable substrates with a constant shear stress state in the adhesive layer (Figure 3). The adhesive shear stress is given by Equation 3 where P is the remote load applied, b is specimen width and l is overlap length. [8, 9]

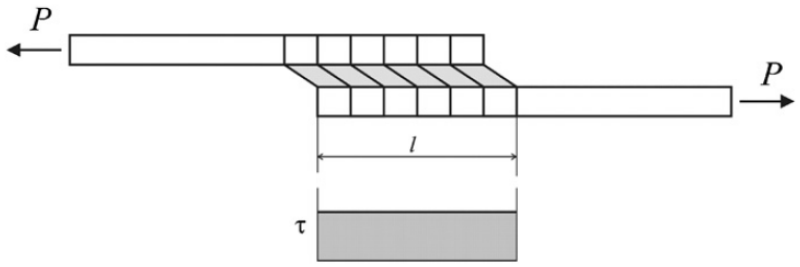

Figure 3 – Deformations in loaded single-lap joints with rigid adherends. [8]

$$\tau = \frac{P}{b \cdot l} \tag{3}$$

b) Volkersen´s analysis

The Volkersen's analysis introduces a differential shear stress in the adhesive as a consequence of substrate deformation (Figure 4). It considers that the SLJ has no bending moment and therefore substrates are in pure tension. The adhesive is in pure shear.[8, 9]

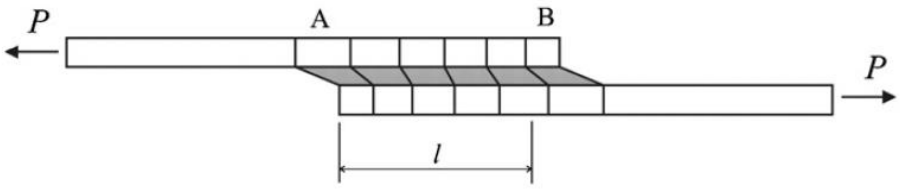

Figure 4 – Deformation in loaded single-lap joints with elastic adherends. [8]

Substrates deformation is maximum near the adhesive overlap (point A) and minimum in the opposite end (point B). The reduction of strain along the overlap causes a non-uniform shear stress distribution in the adhesive (Figure 5).

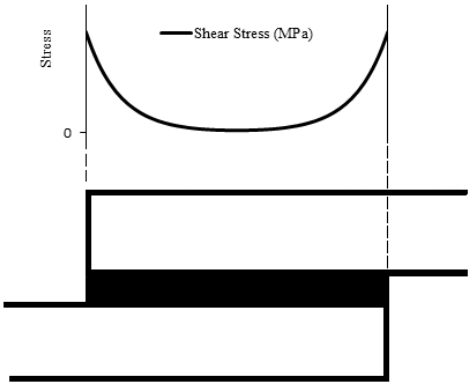

Figure 5 – Typical stress distribution using Volkersen's model for SLJ.

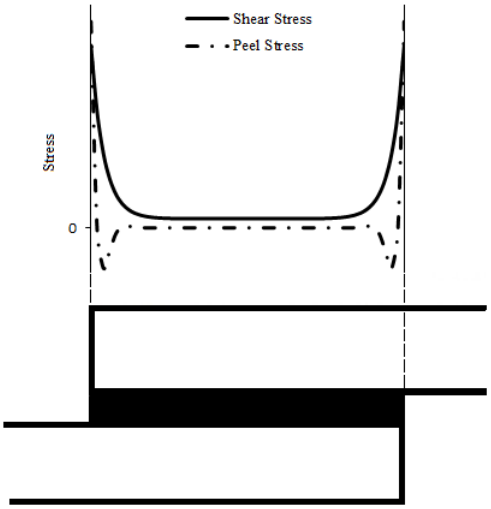

Figure 6 - Typical shear stress and peel stress distribution using Goland and Reissner´s model for SLJ.

The Volkersen´s model does not take into account the effects of the adherend bending and shear deformation, both important aspects for a correct analysis of adhesive joint

stress distribution. This is particularly important in adherends with low shear and transverse modulus.[3, 8, 9]

c) Goland and Reissner analysis

In this analysis a more sophisticated approach is done introducing the aspect of adherend bending and with it peel stresses in the adhesive layer. Figure 6 is an example of the adhesive shear and peel stress in a SLJ. [10]

In summary, the classical analysis of Volkersen and Goland and Reissner were a big step forward in adhesive modelling and failure prediction. Nevertheless there are some limitations to these models. Firstly, variation of stresses along bondline thickness is not taken into account. Secondly, the peak shear stresses at the overlap ends are inaccurate as a correct representation should take into account the zero shear stress at the end of the overlap. Also, the complex stress field of the substrates is neglected to most extend.

In order to improve these models, more work has been done and more complex models have been put forward increasing the accuracy of the stress distributions.[8, 9]

2.2.2 Numerical approach

a) Continuum mechanics approach

In continuum mechanics, one of the approaches is the strength of materials which accounts for the maximum stress and strain. It is among the most used. However it is sometimes inappropriate due to singularities inherent to the bonded joint and in such cases the refinement of the mesh will increase greatly the values obtained from the simulation for the strain and stress. Some common singularities are presented in Figure 7.[3]

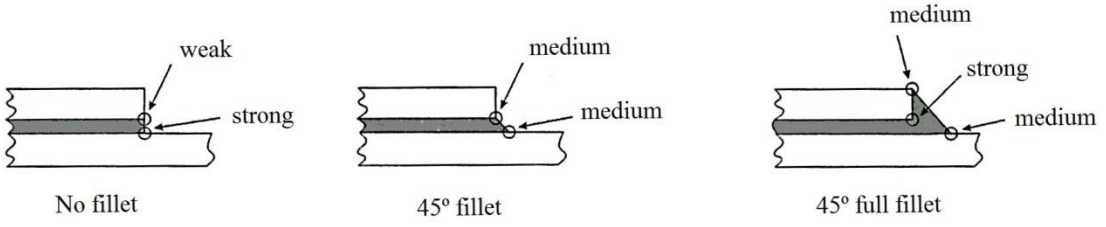

Figure 7 - Examples of singularities in single lap joints and its contribution to the strain and stress results. [3]

b) Fracture mechanics approach

In the continuum mechanics approach, materials are considered to have no defects, in contrast with fracture mechanics analysis where a defect has to exist. The fracture mechanics approach studies the defects to predict if they will cause a catastrophic

failure of the structure or if they can withstand the stresses throughout the service life of the component. In this analysis there are two types of criteria, stress intensity factor and energetic concepts. [11]

It´s a relatively recent field of study and current research is being done to introduce time dependent effects such as viscoelasticity. These effects are important when traditional fracture mechanics are insufficient to accurately predict failure. In this case new computer aided technologies are emerging. [11]

In the traditional approach to the design of structures there are two variables, applied stress and strength of the material but with the introduction of the failure criteria of fracture mechanics this has changed. Following the fracture mechanics approach one takes into account the stress, the flaw size and the fracture toughness of the material. The combinations of these three factors can be done with the energy criterion or the stress-intensity one.[5, 11]

There are three modes of loading that produce a singularity at the crack tip (Figure 8).

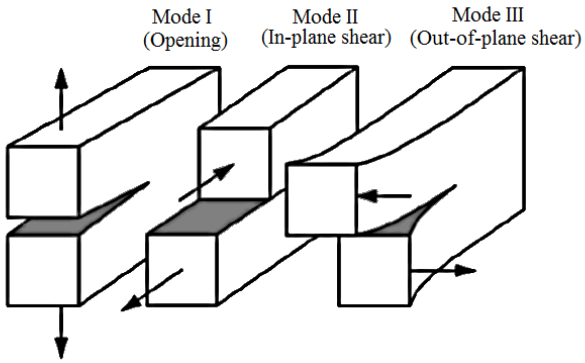

Figure 8 – The three modes of loading that can be applied to a crack.

Energy criterion

The energy approach states that fracture will occur when the energy available for the crack growth is sufficient to overcome the resistance of the material. The material resistance can take into account the surface energy, plastic work, or other energy dissipation associated with the propagation of the crack.[11]

The present version of the approach was developed by Irwin which is defined as the rate of change in potential energy with the crack area for a linear elastic material. At the moment of fracture $G_I = G_{IC}$ (critical energy release rate which is a measure of fracture

toughness). As an example of the method, for a crack of length 2*a* in an infinite plate subject to a remote tensile stress, the energy release rate is given by:

$$G_I = \frac{\pi\sigma^2 a}{E} \tag{4}$$

Where *E* is Young's modulus, σ is the remotely applied stress, and *a* is the half-crack length.[11]

Since a well-designed adhesive joint will fail cohesively, it is reasonable to assume that the fracture toughness is, to some extent, dependent on the adhesive bulk toughness. The fracture toughness is an important aspect of design and has a great variation as a consequence of temperature, geometry and material. Most adhesives are polymers with intermediate fracture toughness and, in most cases, are one order of magnitude lower than the metal and alloys (Figure 9).

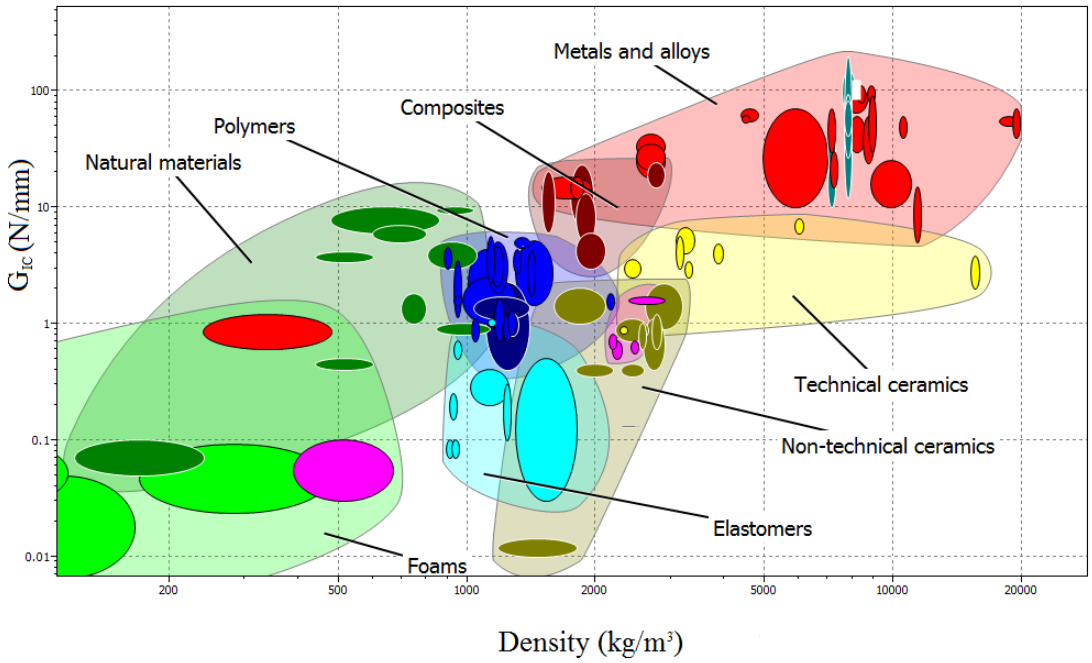

Figure 9 - A comparative representation of the fracture toughness of different materials as a function of density (CesEdupack® (Cambridge, UK)).

Stress intensity approach

According to this criterion one assumes the material will fail locally at a critical combination of stress and strain commonly known as the critical intensity factor, K_{IC}. For a situation similar to the energy approach presented above, infinite long plate subject to a remote tensile stress:

$$K_I = Y\sigma\sqrt{\pi a} \quad (5)$$

Where Y is a correction coefficient to account for structure geometry. In this case K_I is a measure of the local stress and K_{IC} is a measure of the material resistance. The critical stress intensity factor, K_{IC}, is assumed a size-independent material property and can be related to G_{IC}. In the case of plane stress it is calculated through the expression bellow.[11]

$$G_I = \frac{K_I^2}{E} \quad (6)$$

For plane strain:

$$G_I = \frac{K_I^2(1-\nu^2)}{E} \quad (7)$$

c) Cohesive damage modelling

For a cohesive damage analysis no initial crack is needed and its propagation is the result of a simulated degradation of the material. The introduction of the FEA in conjunction with the cohesive mixed-mode damage model is a combination of both continuum and fracture mechanics by including both the strength and the energy parameters to characterize the debonding process. [10]

It is possible to characterize the cohesive zone parameters experimentally using DCB and ENF tests and to incorporate it in a numerical analysis. The results have been very satisfactory and it is possible to predict with accuracy the behaviour of adhesive joints.[3] Different laws for the cohesive zone have been put forward (Figure 10). The cohesive damage model based on the trapezoidal law accounts for the ductile behaviour of the adhesive. For very brittles adhesive both triangular and exponential law are of interest.[10]

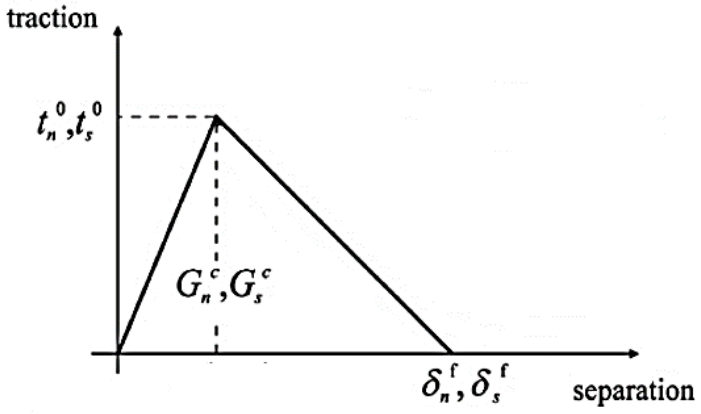

Figure 10 (continues)- CZM laws with triangular, exponential and trapezoidal shapes. [10]

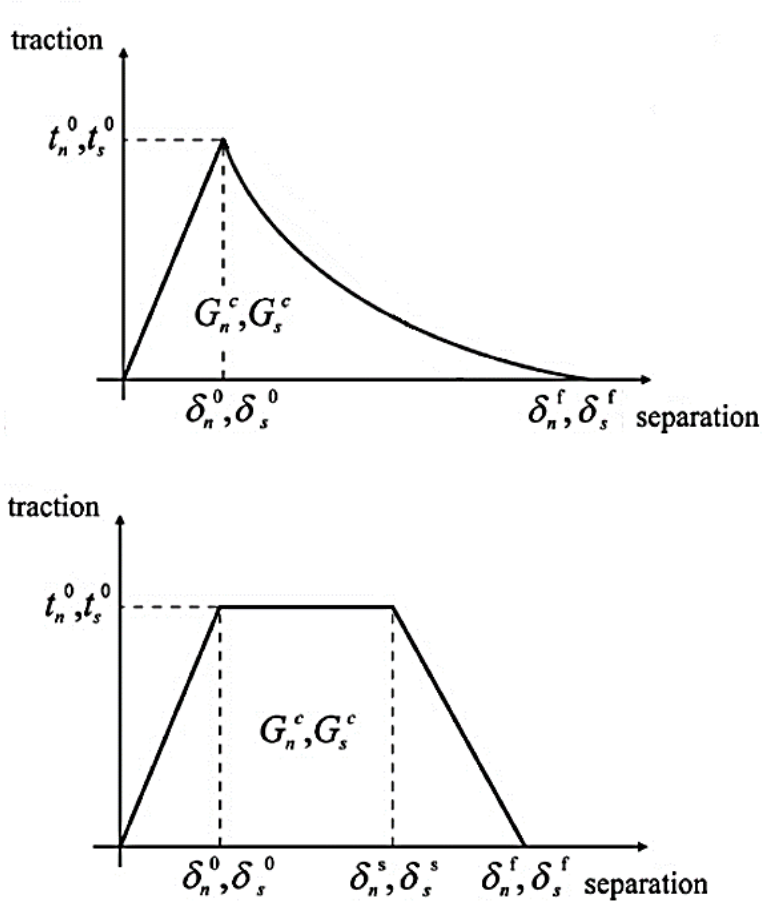

Figure 10 (continued)

2.3 Test methods

2.3.1 Tensile tests

a) Bulk specimens

A common test to determine the strength of the adhesive is the tensile test similar to those for plastic materials. The properties are intrinsic to the material and are obtained under a uniform and uniaxial state of stress. Using this method one can obtain the Young´s modulus, the yield and tensile strength, and elongation at break.

It is usual to obtain the specimens through pouring or injection. The first is suited to one-part adhesives that are liquid. The second gives better results when the adhesive is viscous.[1]

b) Axially loaded butt joints

The tensile properties can also be measured using a thin layer of adhesive between two steel substrates. Many standards exist for this test and round (Figure 11) and square

geometry can be employed. Alignment and adhesive thickness can be controlled using the mold present in ASTM D 2095. [1]

The tensile strength of the adhesive is calculated dividing the load to failure by the initial cross sectional area of the specimen. Also, the adhesive displacement can be measured with an extensometer but a correction has to be made. The influence of the substrates has to be taken into account in order to accurately calculate the adhesive displacement. [1, 12]

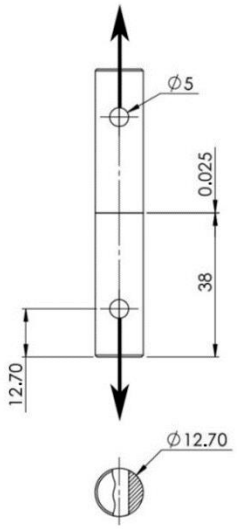

Figure 11 – Butt joint geometry with the load direction (dimensions in mm) (ASTM D 2095)

The stress strain curve is not representative of the intrinsic adhesive behaviour and cannot be correlated with the bulk tensile test. Also, despite the use of precise apparatus and specially designed extensometer, the reproducibility of this test is low. [1, 12]

2.3.2 Fracture strength tests (Mode I)

a) Fracture tests on bulk specimens test

There are several international standards for the determination of the experimental fracture toughness of the bulk specimen, e.g.: ASTM D5045-99 (2007) and ISO 13586:2000. The dimensions for the bulk specimens presented in Figure 12 are chosen to ensure a case of plane strain. For most epoxies the dimensions chosen for SENB are: 6.4 mm thick, 12.7 mm wide, and 75 mm long specimen and it is important to introduce a sharp crack in the specimens in order to have an accurate result of the fracture toughness. This effect is usually accomplished tapping on a sharp razor blade, previously immersed in liquid nitrogen, or by fatigue cracking. [1]

To test SENB specimens a three-point bending fixture is used. Once positioned, the machine records the load and displacement using a constant speed (10 mm/min). Very strict restrictions for the validation of the test exist specially on linearity of the load – displacement diagram.

Using these methods if the amount of plastic deformation is significant an elastic-plastic fracture approach is more appropriate, e.g.: J-integral.[1, 12]

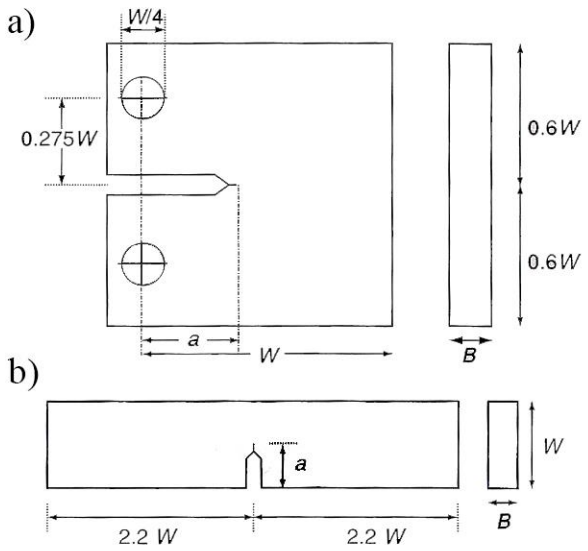

Figure 12 –Fracture bulk specimens, a) compact tension (CT), b) single-edge notched bending (SENB) [1]

b) Double cantilever beam (DCB) test

The specimen geometry is presented in Figure 13 and the loading is done vertically introducing a mode I fracture in the adhesive layer of the DCB specimen.

Two different standards exist, ASTM D3433 and ISO 25217. The first determines the fracture toughness through several loadings of the specimen. This is done in order to induce crack propagation and measure the peak load required, also the load for crack arrest is recorded and the final crack length measured. Both load values are used to measure the fracture toughness.

In standard ISO 25217 the specimen is loaded with a constant cross head displacement up to crack propagation starts. Usually the crack increases slightly, 2-5 mm, and at this point the machine is reset. This pre-crack is not part of the test but a prerequisite. Subsequently the specimen is reloaded again and the resistance to crack initiation and steady-state propagation are calculated.

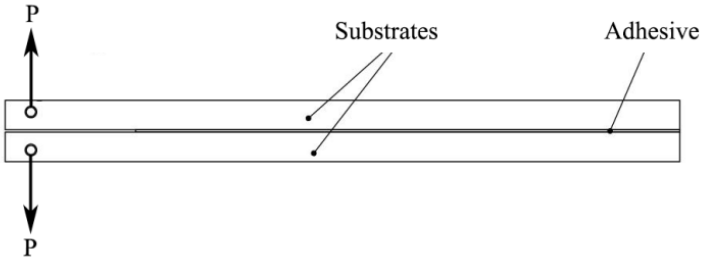

Figure 13 – Mode I double cantilever beam (DCB) adhesive-joint specimen.

Several methods exist to measure the fracture toughness of the DCB test specimens.

Compliance Calibration Method (CCM)

This technique is based on Irwin proposed energy approach defined as energy release rate. The Equation 8 derives from Irwin-Kies theory where G_{IC}, represents the energy available for an increment of crack extension. [11]

$$G_{IC} = \frac{P^2}{2b}\frac{dC}{da} \tag{8}$$

In the above equation P is the load, b represents the width of the specimen on the transversal direction, C is the compliance and a is the crack length.

The partial derivative of the compliance as a function of crack length is obtained from experimental observation of the crack length and the Equation 9.

$$\mathrm{C} = \frac{\delta}{\mathrm{P}} \tag{9}$$

The values are fitted into a cubic polynomial approximation being the compliance, C, a function of crack length, a.

Finally, the cubic polynomial fitting of compliance as a function of crack length is derived and used in the initial equation of Irwin- Kies, Equation 8.

Corrected Beam Theory (CBT)

As a complement, another model was employed. This second model, corrected beam theory (CBT), is an improvement of the CCM and also derives from Irwin-Kies equation. Often, the loading line displacement deviates from the one assumed in the CCM because of the deformation around the crack tip. In this case, the fracture toughness is calculated through:

$$G_{IC} = \frac{3P\delta}{2b(a + |\Delta|)} \tag{10}$$

where Δ is a correction for crack tip rotation and deflection, proposed by Wang and Williams [22], and is calculated using the Equation 11.

$$\Delta = h\sqrt{\frac{1}{13k}\left(\frac{E_x}{G_{xy}}\right)\left(3 - 2\left(\frac{\Gamma}{1+\Gamma}\right)^2\right)} \tag{11}$$

where E_x and G_{xy} is the longitudinal normal and shear modulus of the substrate, h is the substrate's thickness and k is the shear stress distribution constant for correcting the deflection caused by shear force (derived as 0.85 for the DCB specimen).

$$\Gamma = \frac{\sqrt{E_x E_y}}{kG_{xy}} \tag{12}$$

Finally, E_y is the Young´s modulus of the substrates on thickness the direction.[23]

Compliance-Based Beam Method (CBBM)

Although in other methods crack length measurement is necessary, here, by using the crack equivalent concept (Figure 14) this measurement is irrelevant depending only on the specimen's compliance during the test. [24]

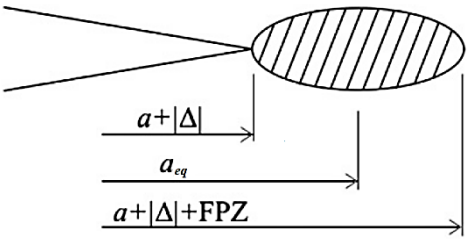

Figure 14 - Schematic representation of the FPZ and crack equivalent concept.

The equation to calculate G_{IC} is [15, 25]:

$$G_{IC} = \frac{6P^2}{b^2 h}\left(\frac{2{a_{eq}}^2}{h^2 E_f} + \frac{1}{5G_{xy}}\right) \tag{13}$$

where a_{eq} is an equivalent crack length obtained from the experimental compliance and accounting for the fracture process zone (FPZ) at the crack tip, E_f is a corrected flexural modulus to account for all phenomena affecting the *P*-δ curve, such as stress concentrations at the crack tip and stiffness variability between specimens, and *G* is the shear modulus of the adherends. [26]

E_f can be obtained using:

$$E_f = \left(C_0 - \frac{12(a_0 + |\Delta|)}{5bhG_{xy}} \right)^{-1} \frac{8(a_0 + |\Delta|)^3}{bh^3} \quad (14)$$

The crack equivalent concept is:

$$a_{eq} = \frac{1}{6\alpha} A - \frac{2\beta}{A} \quad (15)$$

where the coefficients are:

$$\alpha = \frac{8}{bh^3 E_f} \; ; \beta = \frac{12}{5bhG_{xy}} \; ; \; \gamma = -C \quad (16)$$

$$A = \left(\left(1 - 108\gamma + 12\sqrt{3\frac{(4\beta^3 + 27\gamma^2\alpha)}{\alpha}} \right) \alpha^2 \right)^{1/3} \quad (17)$$

Effect of adhesive layer

If the bondline thickness is too low for full development of a plastic zone the fracture toughness will change. As a recommendation, the thickness should be between 0.1 mm and 1 mm. This is also applicable in the case of TDCB. [1, 12]

c) Tapered double cantilever beam (TDCB) test

This method was developed to enable long term measurements of adhesive damage propagation without the need to measure the crack length. The height of the beam changes along the adhesive layer to ensure a constant change of compliance as a function of crack length (Figure 15).[1]

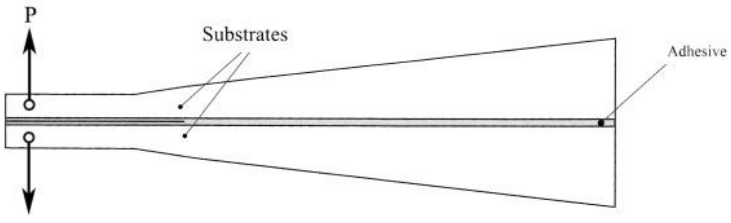

Figure 15 – Mode I tapered double cantilever beam (TDCB) test specimen.

The manufacturing of these specimens is more expensive and complex, requiring a CNC machine to account for the non-linear height profile.

Values of G_{IC} can be determined using a simple beam theory, Equation 18.

$$G_{IC} = \frac{4P^2 m}{E_s b^2} \tag{18}$$

Where P is the load, E_s the substrate elastic modulus, b the substrate width, and m the geometry factor defined previously.

Or using a more complex but accurate method, corrected beam theory. This method formulation is presented below.

$$G_{IC} = \frac{4P^2 m}{E_s b^2} \cdot \left(1 + 0.43\left(\frac{3}{ma}\right)^{\frac{1}{3}}\right) \tag{19}$$

2.3.3 Impact tests

The impact is an important feature when designing an adhesive joint for the automotive industry due to the passenger safety regulations and manufacturer quality standards. As a result the behaviour of adhesive joints in high strain rates is a major consideration in order to know how the strength of the joint reduces varies.

a) Instrumented pendulum impact test

An instrumented pendulum was developed by Harris and Adams to impact a single lap joint or a solid adhesive specimen. The fixture is presented in Figure 16 showing the specimen clapped to the machine's piezoelectric force transducer that in turn is connected to the frame. The other end is free although there is a journal bearing block to guide the specimen during the test. [12]

The strength of the joint is calculated with the load cell and the energy is measured from the pendulum swing after impact. The movement of the end clamp can be instrumented to record the acceleration and thus monitor the position recording the specimen's behaviour.

The energy absorbed by the adhesive rupture is small compared to the energy required to deform the metallic substrates. On the other hand, a low ductility adhesive can have high lap shear strength when using high yield strength substrates and fail with low load loads with ductile substrates.

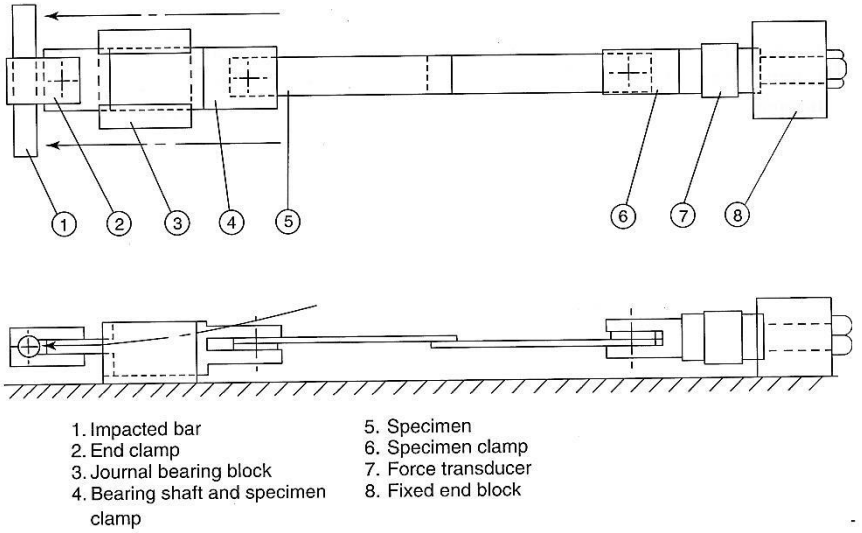

Figure 16 - Instrumented impact pendulum test. [12]

b) Block impact test

This test applies a condition of impact loading, mainly shear, on the test rig similar to that of the Izod resilience measurement (Figure 17). The specimen is fabricated using two blocks, a larger block that will be attached to the base and a smaller block on top of the adhesive layer. This smaller block will be struck during the test by a pendulum in a direction parallel to the bonded surface.

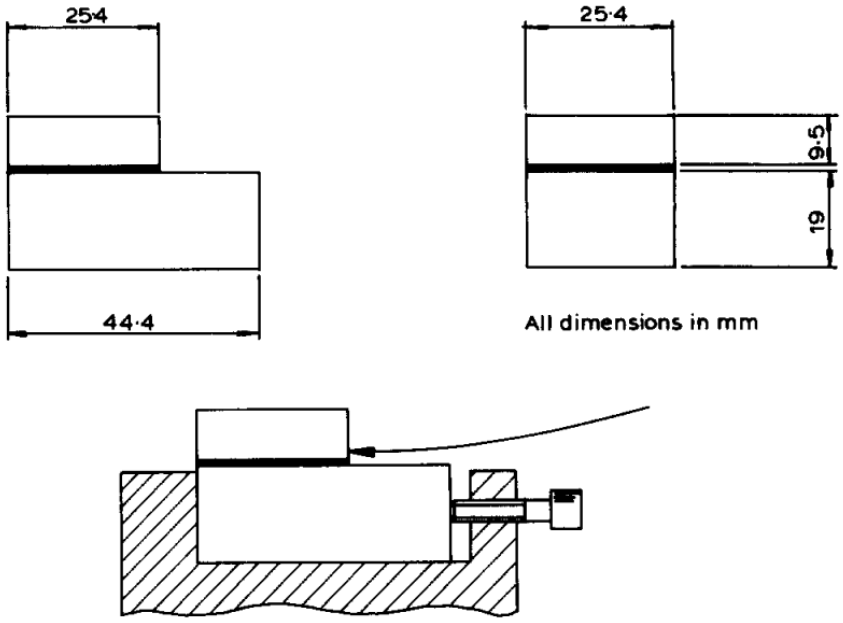

Figure 17 - ASTM block impact test (ASTM D950-78) [12]

In the case of misalignment, the distribution of the shear and peel stresses is strongly influenced. Also, the elastic energy of the steel block may not be negligible in some cases. For these reasons this method is not suitable for the measurement of the energy absorption of the adhesive and can only be used for comparative studies.

c) Impact wedge-peel test

Impact wedge peel test is a realistic test on an adhesive joint with two ductile adherends bonded together to form a Y shape. The two strips used are 90 mm long, 20 mm wide and the thickness can range from 0.6 to 1.7 mm. The bonding length is 30 mm without pre-cracking or crack initiator.

The impact is applied to the shackle, Figure 18, with a pendulum and test is conducted with a speed of 2 or 3 m/s.

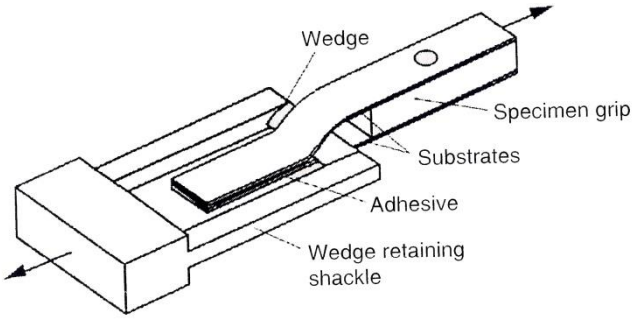

Figure 18 - ISO 11343 wedge impact peel test specimen. [1]

There are usually two different behaviours of adhesive joints when tested with this apparatus, stable or unstable crack propagation. In the first the crack grows more rapidly than the speed of the wedge and is typically encountered when testing at low temperatures or brittle adhesives. In the second case, the crack tip grows ahead of the wedge with a constant offset. In this last case the force-time history exhibits an initial peak, sudden impact and crack initiation, followed by a plateau where it is possible to calculate the cleavage force.

3. Failure strength tests

3.1 Bulk tensile test

3.1.1 Adhesives

The epoxy adhesive XNR6852 was used, supplied by NAGASE CHEMTEX® (Osaka, Japan). This adhesive is a one-part system that cures at 150 ºC for 3 h. This adhesive has a linear structure, which allows greater freedom of movement to the chains, unlike the network structure of a conventional epoxy adhesive. Along with the development of this adhesive, NAGASE CHEMTEX® has produced others with the same technique. The epoxy resin of XNR6852, when pure, is a conventional thermosetting resin due to generating cross-linking during polymerization. A technological advance in the epoxy adhesive has been done and a no cross-linking polymer has been produced through the introduction of phenols. Thus, the reaction process is changed and in this new process the epoxy resin and phenol are polymerized linearly by a consecutive reaction getting a no cross-linking polymer. As a consequence, this polymer has some features of thermoplastic polymers due to the resulting linear structure [18].

Also, the epoxy adhesive SikaPower 4720 was used, supplied by SIKA® (Portugal, Vila Nova de Gaia). This adhesive is a two-part system that cures at room temperature for 24 hours.

3.1.2 Tensile strength test

a) Experimental procedure

Specimen manufacture

The bulk tensile specimens were produced by curing the adhesive between steel plates of a mold (Figure 19) with a silicone rubber frame according to the French standard NF T 76-142. A silicone rubber frame was used to avoid the adhesive from flowing out. The dimensions of the adhesive plate after cure were defined from the internal dimensions of the silicone rubber frame. Then, dogbone specimens were machined from the bulk sheet plates (Figure 20).

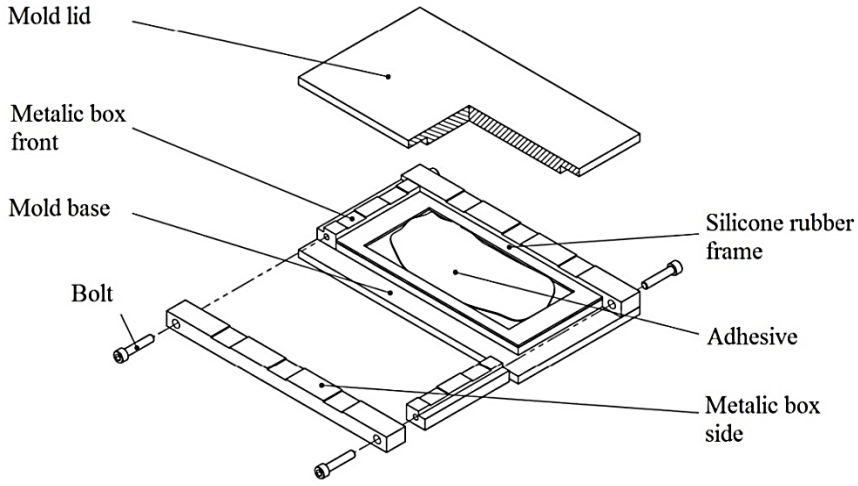

Figure 19 - Exploded view of the mold to produce plate specimens under hydrostatic pressure.

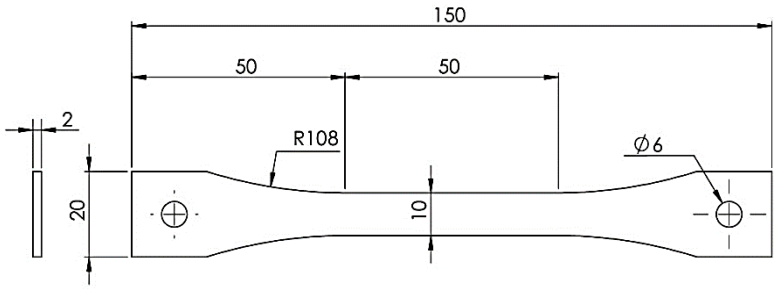

Figure 20 - Dimensions of the bulk tensile specimen used in accordance with standard BS 2782 (dimensions in mm).

Test procedure

The bulk tensile test was performed in an INSTRON® model 3367 universal test machine (Norwood, Massachusetts, USA) with a capacity of 30 kN, at room temperature and constant displacement rate of 1 mm/min. An extensometer to record the displacement was also used. Loads and displacements were recorded up to failure. Four specimens of each were tested.

b) Experimental results and discussion

Figure 21 and Figure 22 present a comparison of a tensile curve between toughened epoxy; AV 119 from Hunstman® [19], a polyurethane (PU); Pliogrip 7400/7410 from Ashland Specialty Chemicals® [20], and the studied adhesives; XNR 6852 and SikaPower 4720. The values of tensile strength determined in this test for XNR 6852 correspond to the values expected for a conventional epoxy adhesive (Table 3). In

contrast the two part epoxy, SikaPower 4720, has a low tensile strength more typical of polyurethane or a natural rubber. On top of it, the maximum strain is small and is far from the 100% strain of XNR 6852. In conclusion, XNR 6852, has a maximum strain much higher than a conventional toughened epoxy adhesive and a higher strength than a polyurethane adhesive.

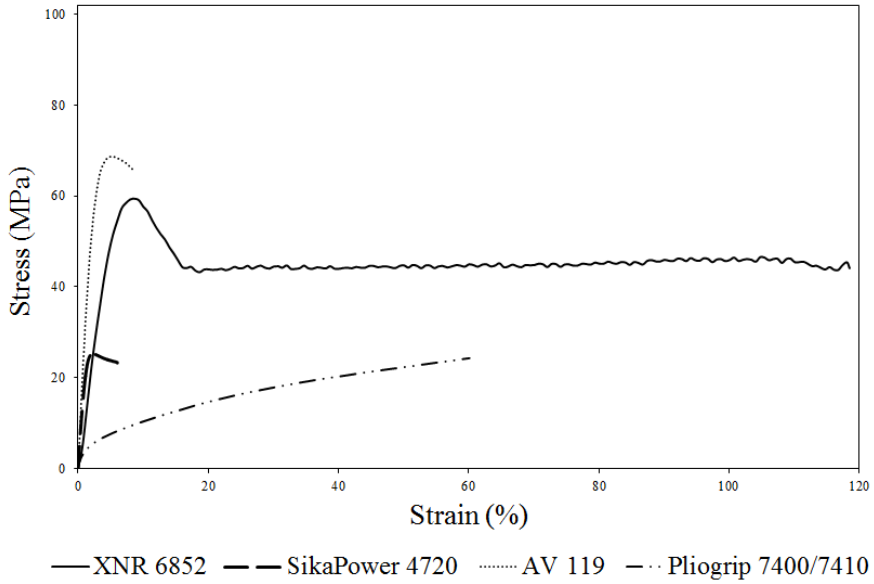

Figure 21 - Stress-strain curve with, Pliogrip 7400/7410 (PU), AV 119 (toughened epoxy), XNR6852 and SikaPower 4720

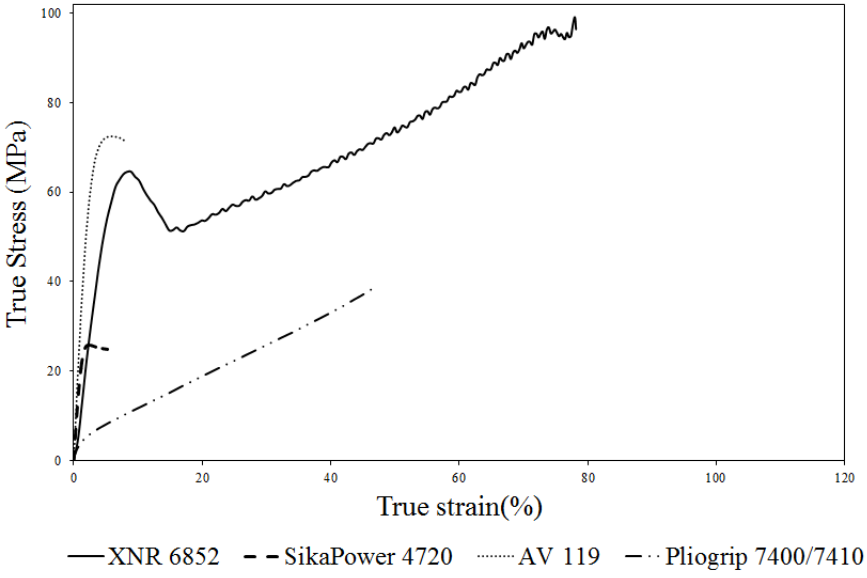

Figure 22 - True Stress-True strain curve with, Pliogrip 7400/7410 (PU), AV 119 (toughened epoxy), XNR6852 and SikaPower 4720.

The stress-strain curves of polymeric materials are not linear in tension and have usually low rigidity in the elastic domain. Despite the evident non-linear behaviour, the

Young´s modulus is used to describe most adhesive as it is simple to determine. It is worth mentioning that the shear modulus is relatively linear.[5]

The Young's modulus obtained for XNR 6852 is approximately half of a typical toughened epoxy (Table 3) and it is a consequence of the addition of the phenols. This property can have some advantages to the vibration damping [21] because of its smaller rigidity. On the other hand, SikaPower 4720 has a normal Young's modulus for a toughened epoxy.

Table 3 - Results of bulk tensile tests

	Tensile strength (MPa)	Young's modulus (MPa)	Strain (%)
XNR6852	59.9±0.84	1176.3±39.9	100.7±25.52
SikaPower 4720	25.0±0.25	2030.9±86.7	4.9±0.79
AV 119	60	2400	3

Before fracturing, adhesive XNR 6852 deforms in a ductile manner (Figure 23, a) suffering a reduction of area and acquiring an opaque colour, behaviour typical of thermoplastic polymers. This behaviour is an improvement in the properties of epoxy adhesives demonstrating an increased ductility of the material. As for the SikaPower 4720, it has a very fragile behaviour with little deformation (Figure 23, b).

Figure 23 – Bulk tensile specimens after test, a) XNR 6852 and b) SikaPower 4720

3.1.3 Optimization of the bulk tensile test specimen

a) Experimental procedure

Specimen manufacture

In order to increase productivity of specimens for the durability project that follows a reduction of specimen size is required. The reason is the many hours that take to cure the adhesive and the low number of long dogbone specimens produced with a single

bulk plate. To produce the short specimens the same manufacturing process as for the long dogbone was employed.

A first attempt was made with standard EN ISO 572-2, short specimen, represented in Figure 24. This geometry is suited for ductile adhesive such as polyurethanes.

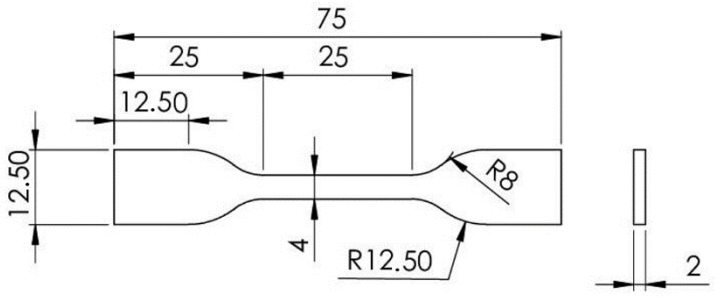

Figure 24 – Short tensile specimen according to EN ISO 527-2 (dimensions in mm)

The geometry in Figure 25 is not in accordance with any standard and was developed with the purpose of eliminating, as far as possible, the concentration of stress. In order to do so, a less abrupt transition was used with higher (double) radius.

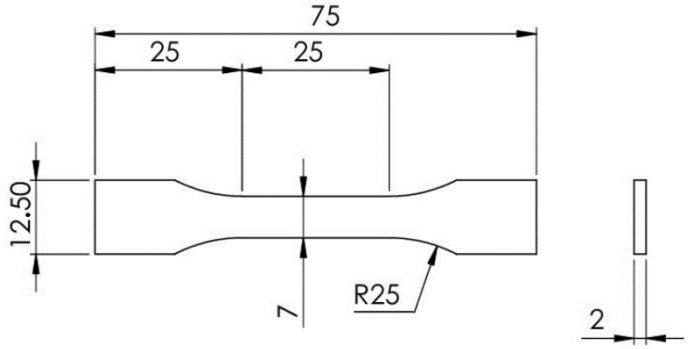

Figure 25 – Short specimen with transition radius of 25 (dimensions in mm)

A further improvement of the previous geometry with an increased radius and increased cross section area was developed. Figure 26 shows the geometry of this specimen.

In all cases, the specimen thickness was 2 mm.

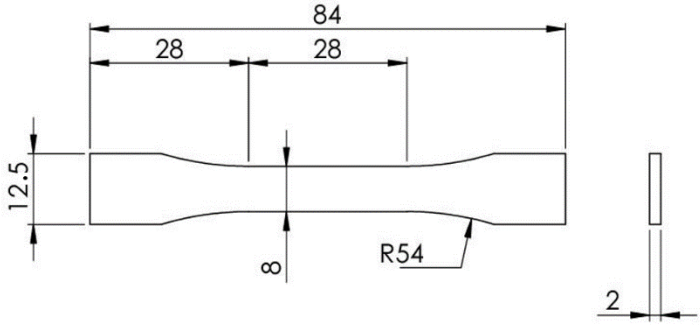

Figure 26 – Short specimen with a 54 radius in the transition area (dimensions in mm)

The introduction of the smaller specimens boosted productivity. On top of that, a steel plate in the middle of the mold introducing a second layer of adhesive increased productivity by a factor of two and also will save many hours of work.

Test procedure

The bulk tensile test was performed in an INSTRON® model 3367 universal test machine (Norwood, Massachusetts, USA) with a capacity of 30kN at room temperature and constant displacement rate of 1mm/min. When testing the first and second geometry no extensometer was used because the specimen was very fragile and would fail due to the sharp edges of the apparatus. Three specimens were tested.

b) Experimental results and discussion

The stress-strain curve of short specimen (EN ISO 527-2 standard) using XNR 6852 is presented in Figure 27. Due to the concentration of stress in the necking area the maximum stress to failure decreased for the short specimen. It is also worth mentioning that although no extensometer was used the Young´s modulus is approximately the same.

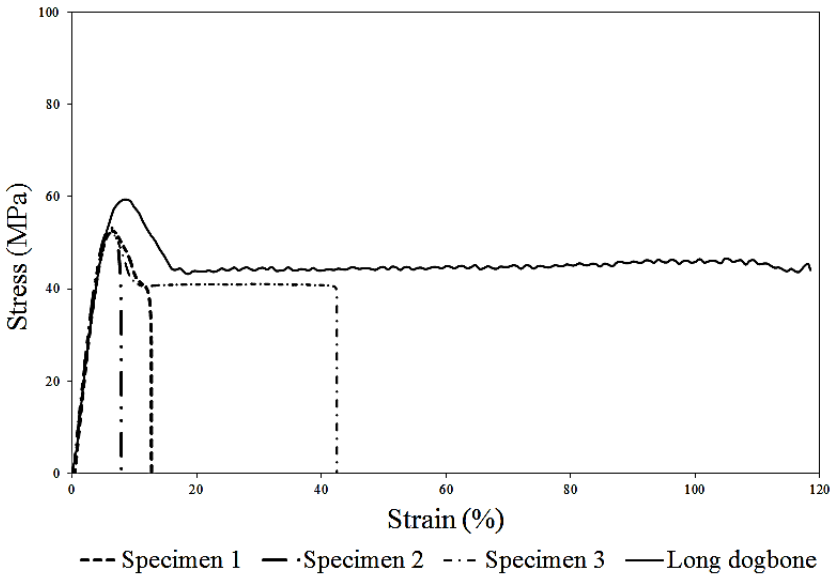

Figure 27 – Comparison of stress and strain curves between the EN ISO 527-2 short specimen and long dogbone specimen using XNR 6852.

Although the specimens with geometry of Figure 24 tested with XNR 6852 had a ductile behaviour (Figure 28) it did not have the same magnitude of elongation as previously with the long specimens. On top of it, it was also very susceptible to machining imperfections and inclusions.

Figure 28 – Ductile fracture of the short specimen (EN ISO 527-2 standard) in the necking part of the specimen using XNR 6852

The results of the short specimen (25 mm radius) with adhesive XNR 6852 are presented in Figure 29. The maximum stress of this short specimen is similar to the long dogbone tested previously. On the other hand, the elongation was much smaller in all cases tested and is the consequence of small flaws in cross sectional area causing sudden failure.

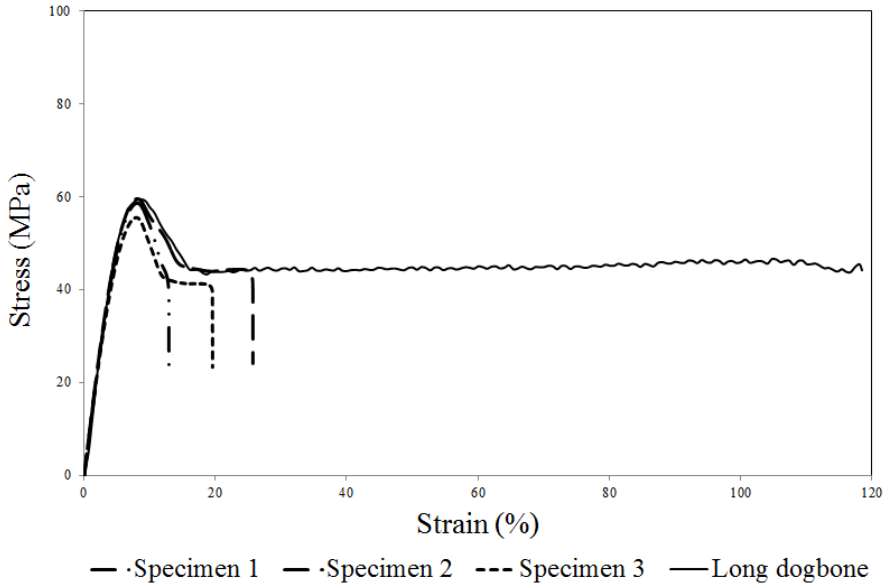

Figure 29 - Comparison of stress and strain curve between the short specimen (25 radius) and long dogbone specimen using adhesive XNR 6852.

The second geometry tested was also very susceptible to imperfections and as a result failed sooner than the long counterpart.

Figure 30 - Ductile fracture of short specimen (25 radius) in the necking part of the specimen using XNR 6852.

In summary, for the ductile adhesive XNR 6852, the stress concentration is not influencing the results and the values necessary for a finite element analysis can be

acquired with the second geometry presented above (Young´s modulus, Tensile strength). However, for a fragile adhesive as SikaPower 4720 the stress concentration can still be relevant.

The stress and strain curves for the SikaPower 4720 are presented in Figure 31. In all cases the tensile strength was only slightly lower than the long dogbone specimens, with a mean of 24.32 MPa ± .12 opposed to 24.96 MPa ± 0.24. In contrast, the maximum elongation was higher in almost all tests.

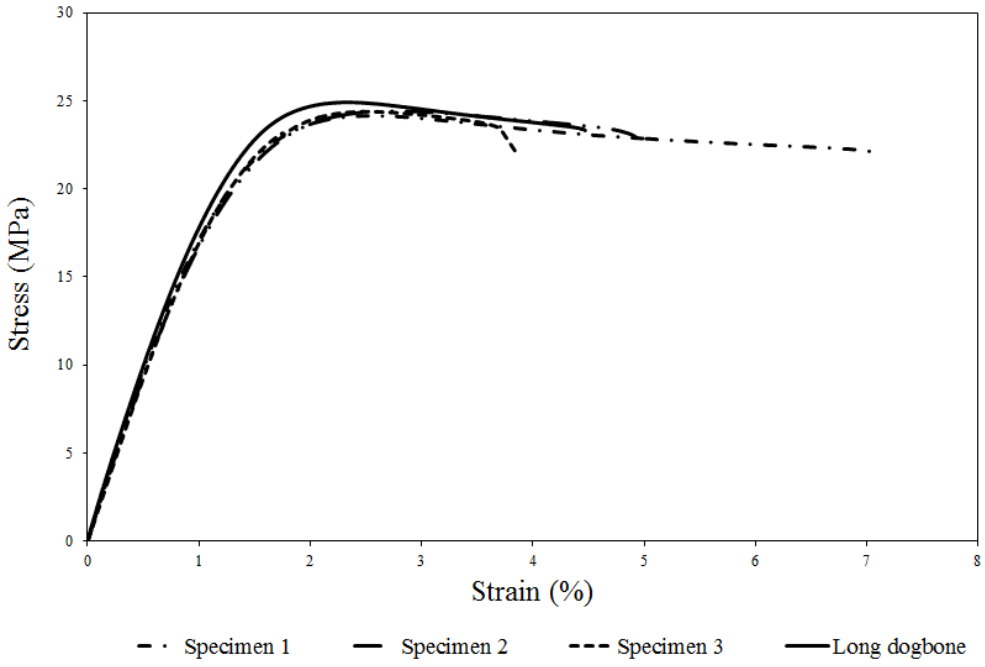

Figure 31 - Comparison of stress and strain curve between the short specimen (54 radius) and long dogbone specimen using SikaPower 4720.

The adhesive SikaPower 4720 tested with the geometry presented in Figure 26 experienced a brittle fracture (Figure 32).

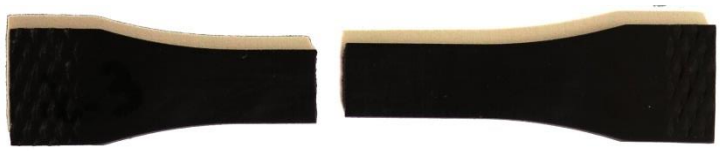

Figure 32 – Fragile fracture of the short specimen (54 radius) using SikaPower 4720.

In summary, the adhesive is a soft material and with the avoidance of the extensometer for small specimens it is granted that there is no damaging of the adhesive being tested. On the other hand, there is a loss of precision and a non-reliable maximum elongation

and Young´s modulus due to the deformation of the machine and the slipping of the specimen. For a proper tensile test, long dogbone specimens are necessary and an extensometer is mandatory.

However, for the durability project, the maximum elongation does not have any influence on the models for it is accounted for using the fracture toughness. So, using the geometry of the short specimen with 54 mm radius a reliable Young´s modulus can be calculated with the use of an extensometer.

Although it is clear that some stress concentration will most likely be impossible to eliminate an improvement of the results for the test specimens was obtained.

c) Numerical results and discussion

Using Abaqus® a linear elastic analysis was performed. A simplification of the geometry was made making use of specimen symmetry. A plane stress case was chosen.

The simulation was run with the Young´s modulus of XNR 6852 taken from Table 3 and a Poisson´s ratio (ν) of 0.4. As a note, for polymeric adhesives, the Poisson's ratio varies between 0.37 and 0.5 being the former for temperatures below T_g and the later above it. For example, hydrocarbon rubbers exhibit a Poisson's ratio of 0.49 and the epoxies show values of 0.37 at room temperature. [1]

After several refinements of the mesh, the stresses in the specimen were analysed and compared. In the specimen a of Figure 33, there is a severe change in stress from the holding part of the specimen and the test area. Furthermore a stress concentration is present near the end of the tangent radius. This effect happens in all three cases.

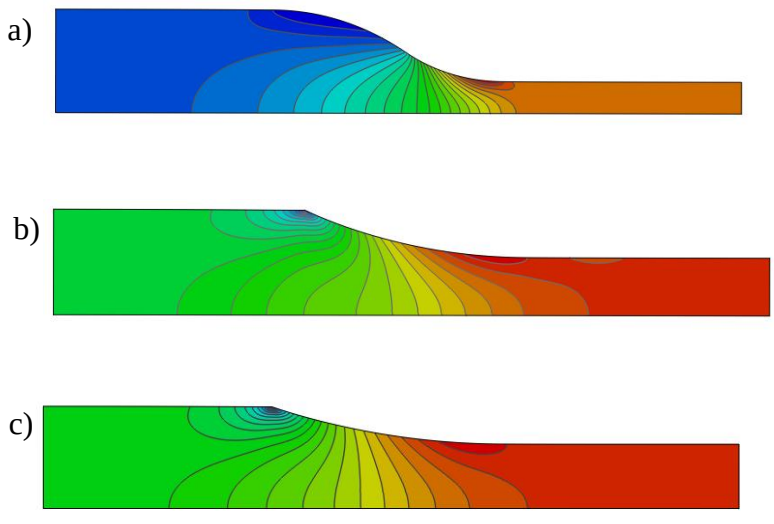

Figure 33 - Principal stress distribution in the horizontal direction (σ_{11}) for the short tensile specimen, a) short tensile specimen according to EN ISO 527-2, b) short specimen with transition radius of 25mm, c) short specimen with a 35 radius in the transition area

The stress concentration factor was calculated using Equation 20 and the results are presented in Table 4.

$$K = \frac{\sigma_{max}}{\sigma_{11}} \tag{20}$$

The specimen c of Figure 33 has the lower stress concentration of the three. In the numerical analysis only the linear elastic phenomenon was studied and as a result one has to assume that in the plastic region stress concentration can be ignored if in the presence of a ductile adhesive.

Table 4 – Comparison of the stress intensity factor between the three cases studied (see Figure 33).

	Case		
	a	b	c
K	1.071	1.043	1.036

4. Fracture tests

4.1 Numerical analysis of the DCB tests

For the durability project a reduced DCB specimen is to be used in order to decrease the diffusion time. Furthermore, the normal DCB specimen is longer than the small chamber used to test at high temperature. Because the toughness results will change due to a different geometry, a study of the influence of these properties was done using a numerical analysis.

4.1.1 Numerical modelling

The numerical analysis was performed in Abaqus® to study the influence of different geometries in the fracture toughness. This was done using two dimensional models and comparing the results to a standard model with the geometry of the specimens commonly tested in laboratory (Figure 34).

Firstly, in Abaqus®, a part was created with the dimensions of the specimen. Afterwards, several partitions were made to improve the mesh construction.

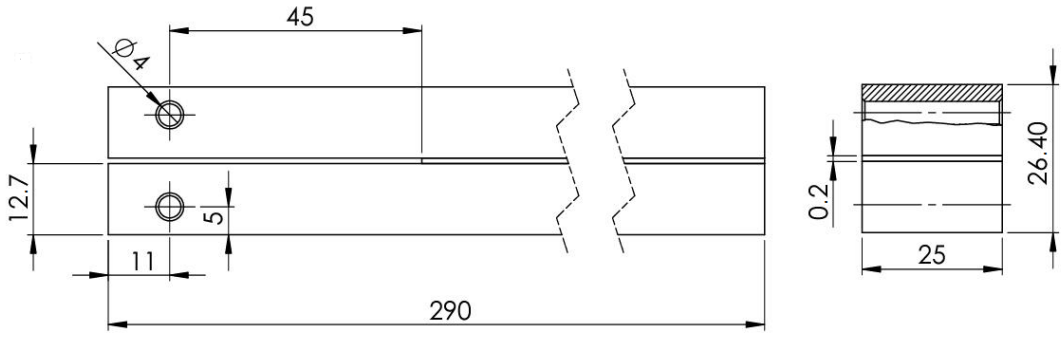

Figure 34 - Geometry of the DCB specimen (dimensions in mm).

The second step was to introduce the properties of the materials (Table 5) in the database and appoint sections. Subsequently, an assembly model was created.

Table 5 - The adhesive properties used for the simulations

	Young´s modulus (MPa)	*Shear modulus (MPa)	Tensile strength (MPa)	*Shear strength (MPa)	G_{IC} (N/mm)	G_{IIC} (N/mm)
XNR6852	1176.3 ± 39.9	823.41	59.9 ± 0.84	37.5	1.97 ± 0.38	12.5 ± 1.1

* Data aquired indirectly from tests

The shear modulus was calculated with Equation 14 using a Poisson's ratio (ν) of 0.4. It is only valid for simple stress fields with no shear.

$$G_{xy} = \frac{E}{2(1+\nu)} \tag{21}$$

A general/static analysis was chosen in the step module library. Also, an output field for the degradation of the adhesive was programed in order to evaluate the adhesive condition. No interactions were input in the program.

The boundary conditions are presented in Figure 35, c).

The specimen arms were modelled with plane-strain 4-node quadrilateral solid (CPE4R: A 4-node bilinear plane strain quadrilateral, reduced integration, hourglass control). In order to have a square cohesive finite element with a 0.2 mm edge, the seed edges function was used. The mesh was constructed taking advantage of the automatic capabilities of Abaqus®.

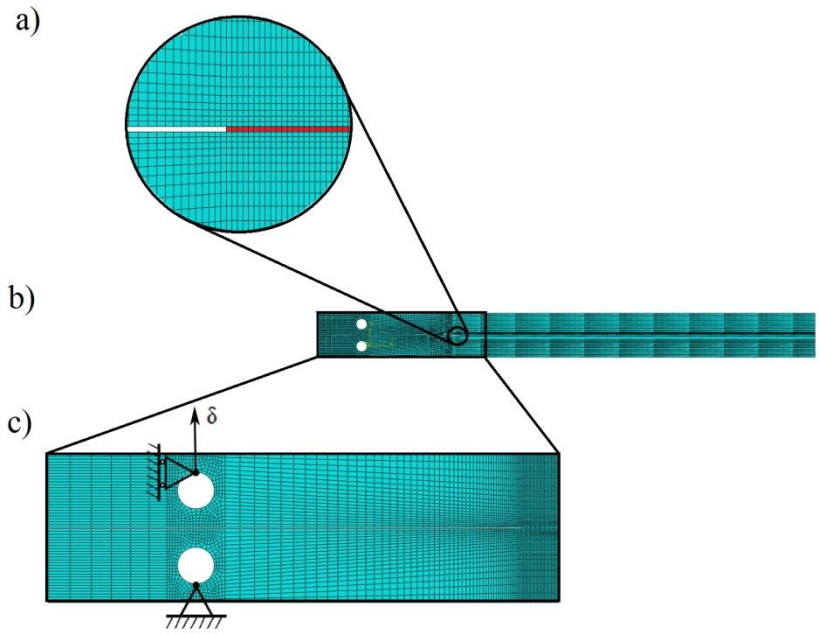

Figure 35 – Modelled DCB specimen with the finite element mesh, a) cohesive zone (red), b) view of the all specimen, c) boundary conditions.

a) Cohesive zone model

The experimental values of toughness and strength present in Table 5 were used to configure the triangular CZM model presented below.

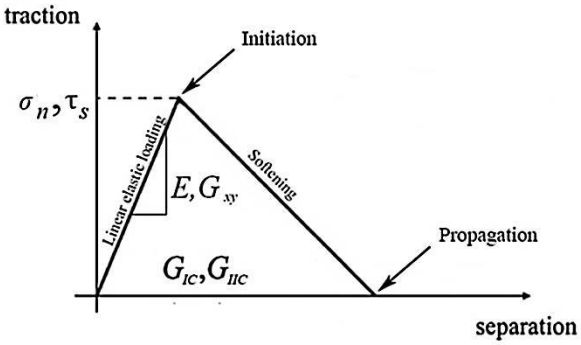

Figure 36 - Traction separation law with linear softening available in Abaqus®

The area under the traction separation law, in both mode I and mode II, is equal to the respective fracture energy. Under pure mode I or mode II, damage propagation occurs at a specific integration when the stress is released in the traction-separation law. Initially it assumes a linear elastic behaviour followed by a linear evolution of damage.

Although it is pure mode I crack propagation, an energy criterion was chosen for mixed mode crack propagation. The linear energetic criterion for complete separation chosen is presented in Equation 22.

$$\frac{G_I}{G_{IC}} + \frac{G_{II}}{G_{IIC}} = 1 \tag{22}$$

b) Data analysis

To calculate the critical fracture energy in mode I, G_{IC}, three different methods were used: Compliance Calibration Method (CCM), Compliance Beam theory and Compliance-based beam method (CBBM).

4.1.2 Numerical results and discussion

a) Initial crack length

Three initial crack lengths were studied to investigate the effect on the toughness measurement. The three initial cracks used in Abaqus® were: 20 mm, 56 mm and 120 mm. The *P-δ* curve presented below shows a high rigidity for the specimen with a short crack, a softer linear loading for the intermediate and a further decrease in compliance for the bigger crack. Also the maximum load for each crack decreased accordingly to the crack length. All the graphs coincide once the crack length is the same.

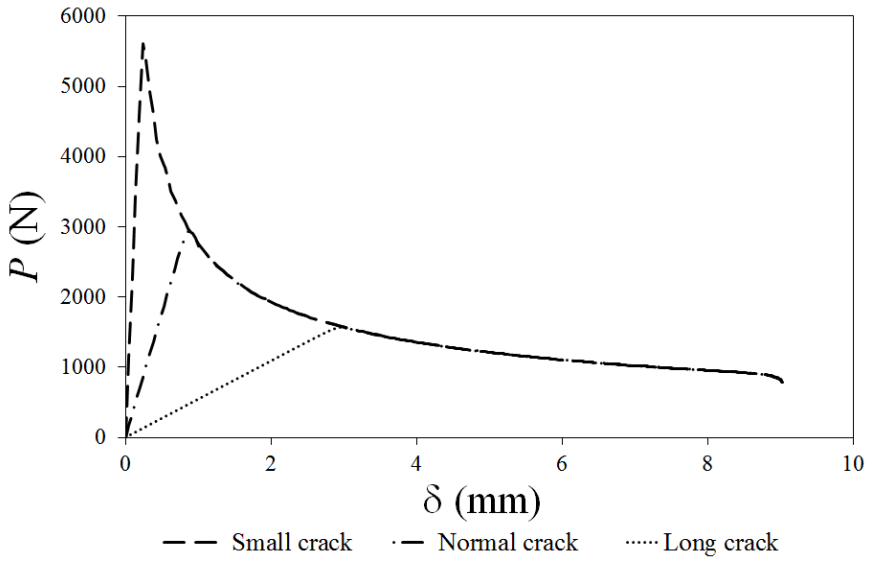

Figure 37 – Numerical P-δ of three different initial cracks.

To complement the *P-δ* curve Figure 38 shows the variation of the applied load with the crack length. Again, for the same crack length the applied load coincides.

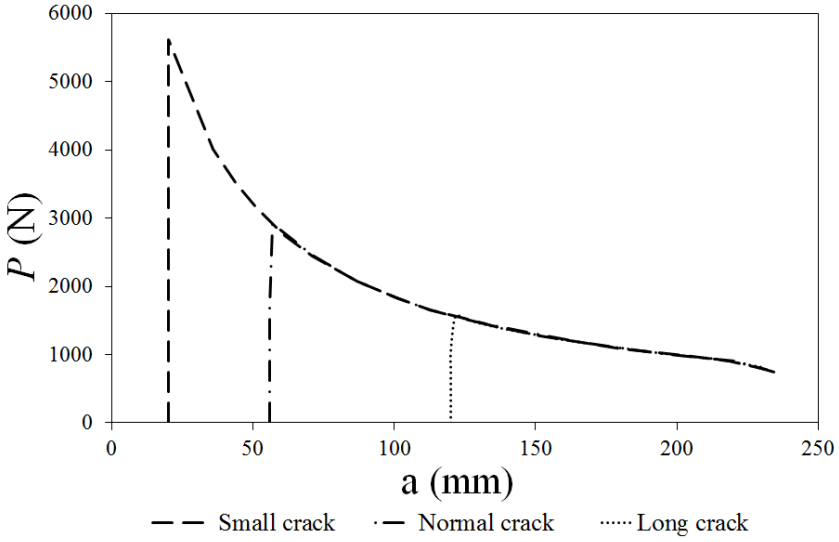

Figure 38 – P-a curve for the three different initial crack lengths.

The R-curves calculated from the numerical data acquired are presented below.

a)

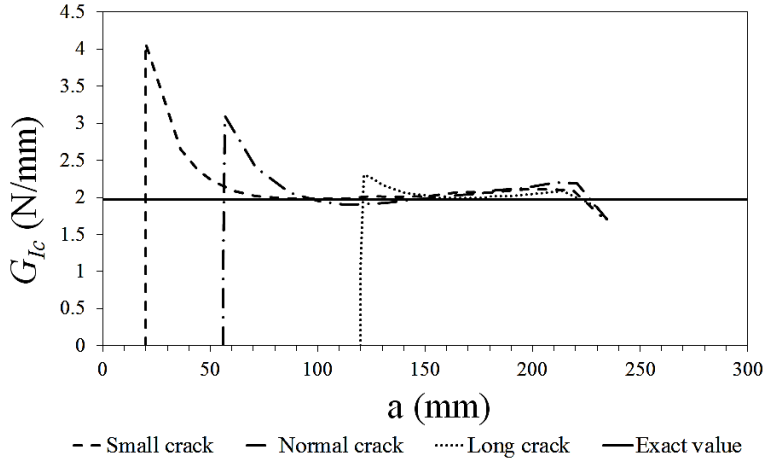

b)

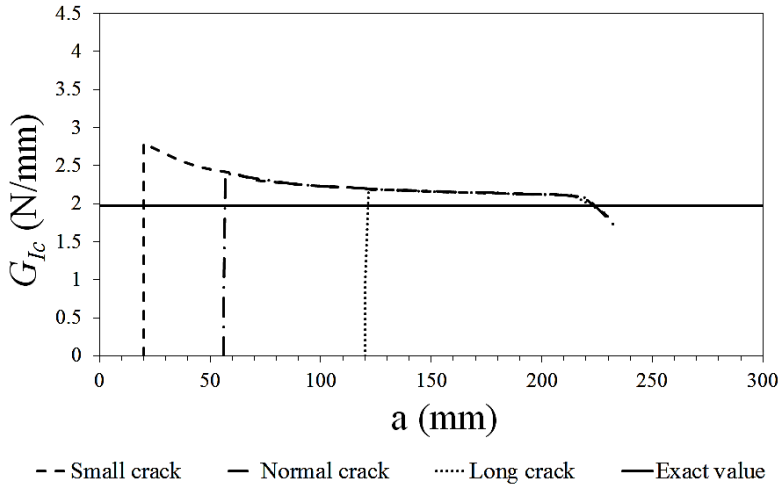

c)

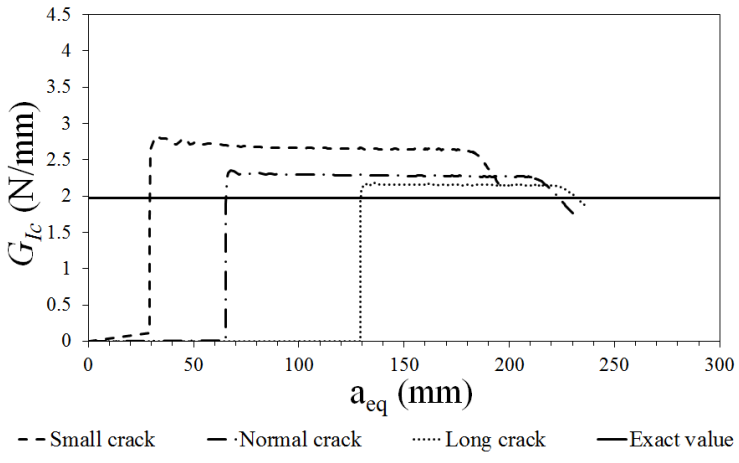

Figure 39 – Numerical R-curves of the three different initial cracks lengths, a) CCM method, b) CBT method, c) CBBM method.

The CCM and the CBT have a peak in the initial toughness (Figure 39). This peak is higher in the CCM method but rapidly tends to the exact value. In contrast the CBT has a smaller peak but a smaller slope until the exact value. Lastly the CBBM is highly

influenced by the initial crack length and, in the plateau region, the value of fracture toughness does not converge.

The fracture toughness was calculated using the plateau region of the R-curve and the results are compiled in Figure 40. From all the methods used the CBBM is the most affected by the initial crack length with an increased toughness. Although CBT has a similar behaviour, it is more consistent and is not affected to the same extend as CBBM method. The accurate method was CCM giving precise results in all three tests with different initial crack lengths.

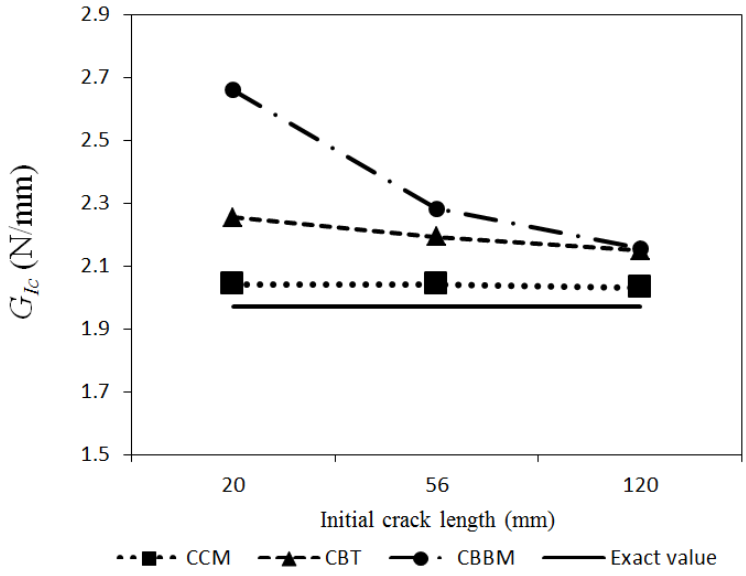

Figure 40 - Summary of the numerical fracture toughness as a function of initial crack length.

b) Specimen length

A crucial parameter is the length of the specimen because the chamber has a limitation of 120 mm from the loading line. As a result, three specimen lengths were used, 290 mm, 240 mm and 200 mm. The *P-δ* curve of the simulation is presented below.

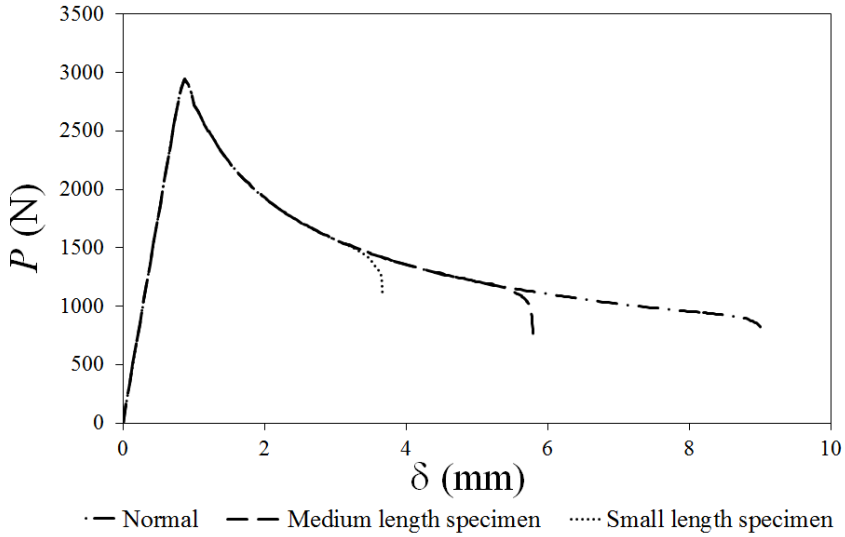

Figure 41 - Numerical P-δ of three different specimen length.

To complement the previous graph, the force versus crack length is presented in Figure 42.

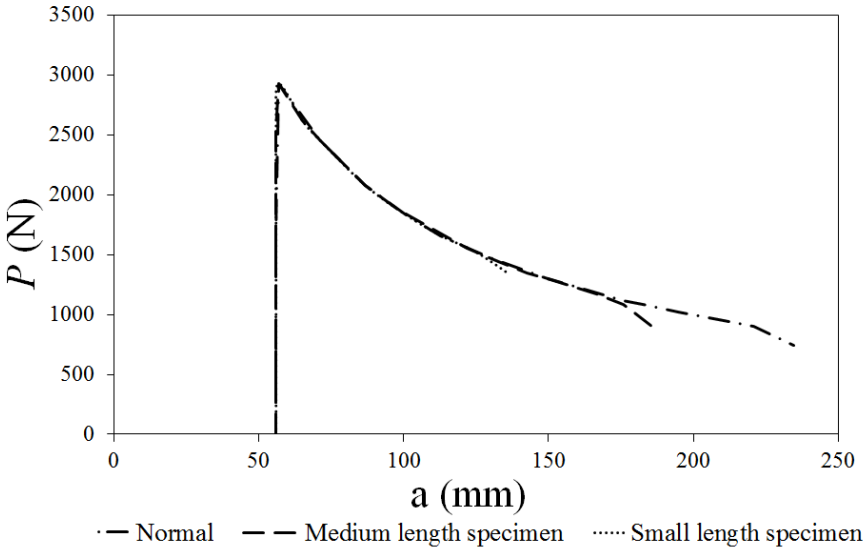

Figure 42 – P-a curve for the three different specimen length.

The results from the Abaqus® simulations are similar and only small variations between the three lengths can be perceived in the Figure 41 and Figure 42.

a)

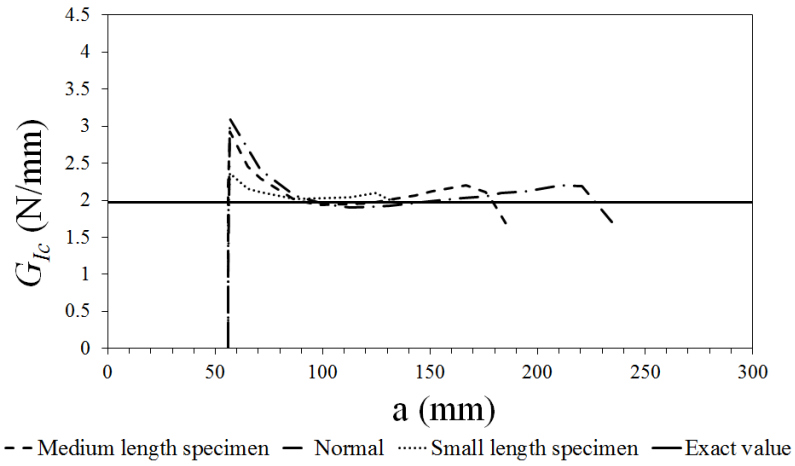

b)

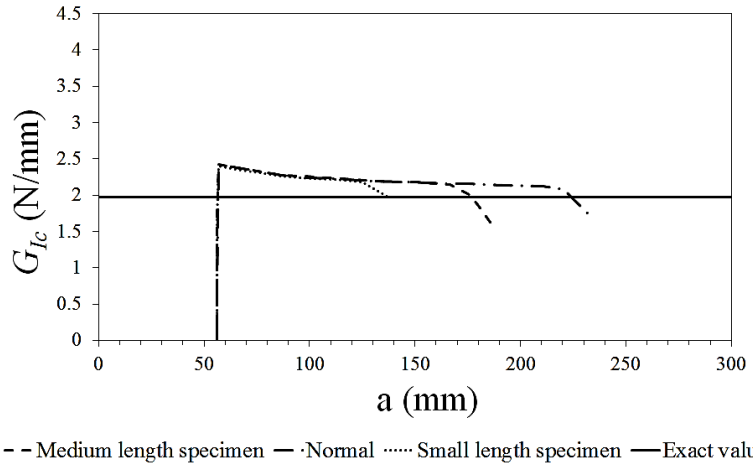

c)

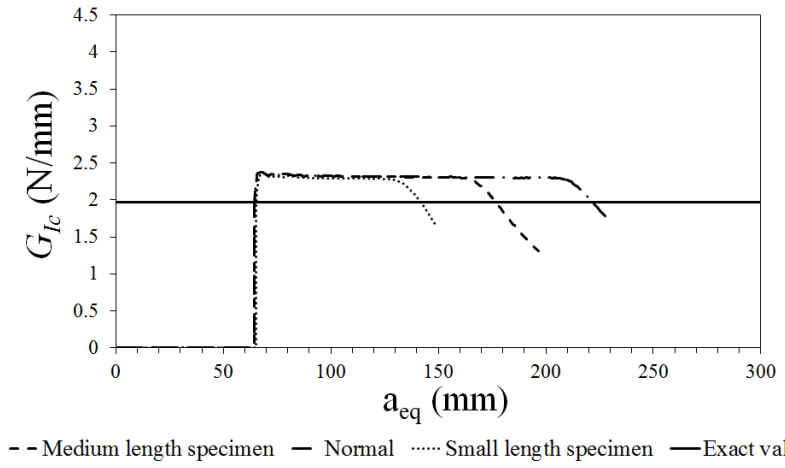

Figure 43 – Numerical R-curves of the three different specimen lengths, a) CCM method, b) CBT method, c) CBBM method.

The results from the CCM method are the only that have a shape with a big deviation from the normal specimen. In the two other methods the difference in the shapes of the R-curves is only due to the breaking of the specimen.

The fracture toughness is in this case almost constant and it can be assumed that there is little influence of this parameter. In conclusion, if it is guaranteed enough length for a stable propagation then the fracture toughness in the plateau region is not influenced by the length of the specimen.

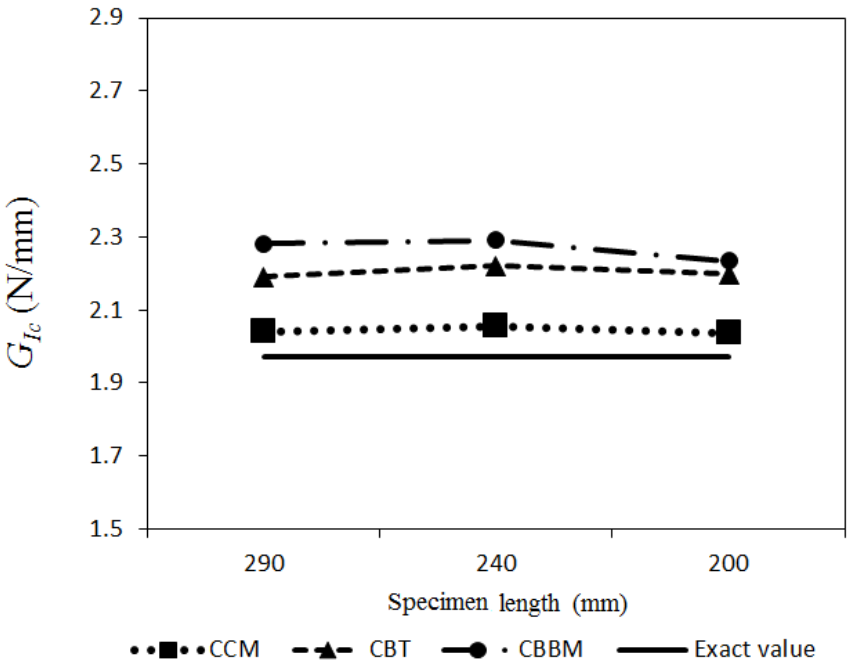

Figure 44 - Summary of the fracture toughness as a function of specimen length.

c) Specimen width

Three different widths were used, 50 mm, 25 mm and 10 mm. The failure load increased proportionally with the width and is consistent with the FEA formulation (Figure 45). In other words, there is no influence in the simulation and the parameters that influence it.

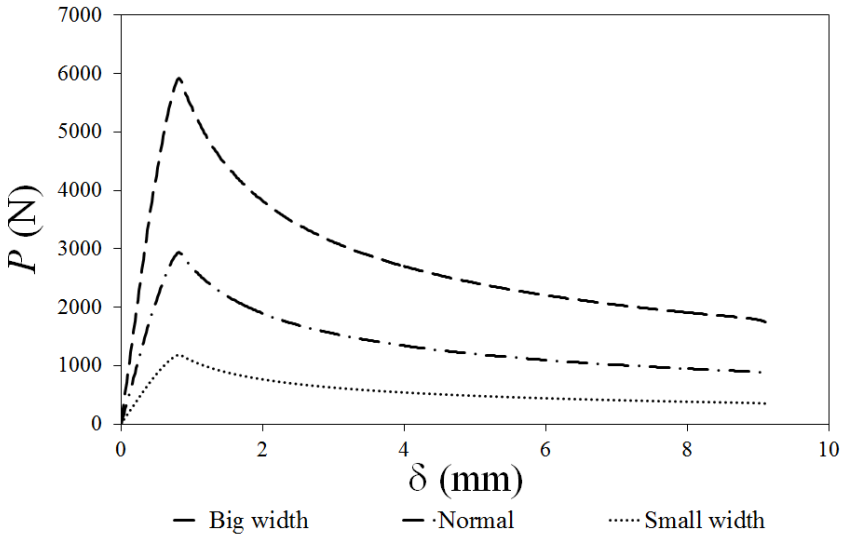

Figure 45 – Numerical P-δ curve for three different widths.

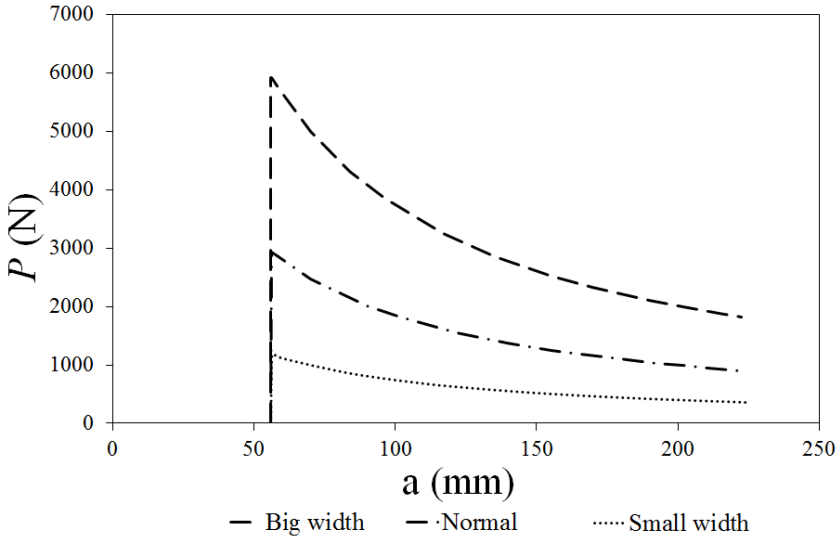

Figure 46 – Numerical P-a curve with three different widths.

In all methods the shape of the R-curves was identical as was the fracture toughness in the plateau region (Figure 47).

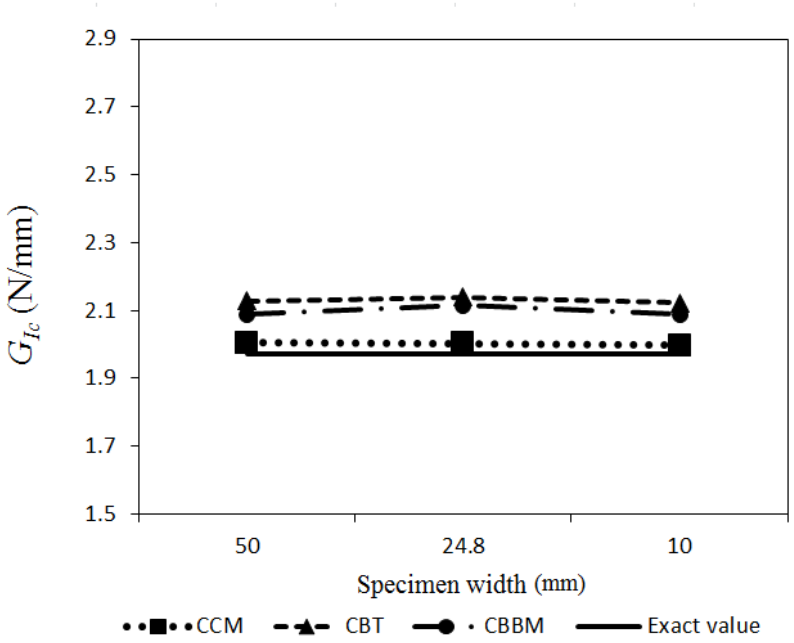

Figure 47 – Comparison of the numerical fracture toughness in the plateau region of the R-curve for three different widths and three different methods: CCM, CBT and CBBM.

The decrease of the width has little influence on the numerical results. However, diffusion in the bondline of the DCB specimen can take up to two years and a reduction of the section can decrease greatly the period of the durability study.

d) Substrates thickness

Three substrates thickness were studied, 15 mm, 12.7 mm and 9 mm.

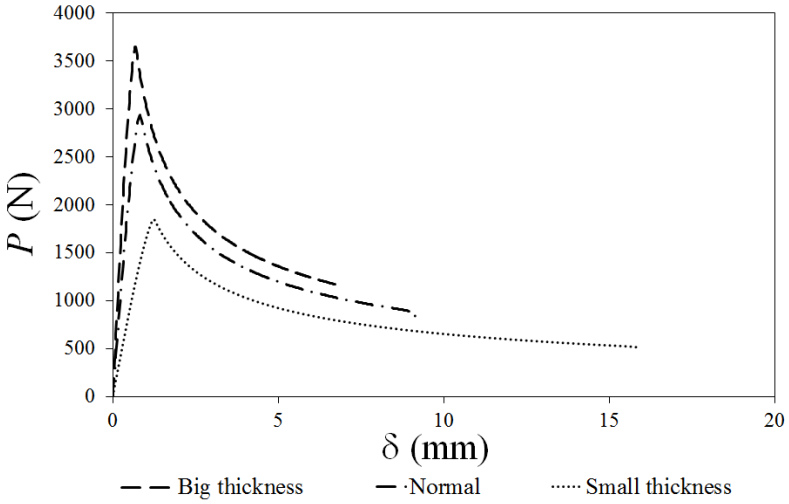

Figure 48 – Numerical *P-δ* curve of three different thicknesses.

Increasing the thickness of the substrates can improve the adhesive´s maximum load (Figure 48 and Figure 49). This is the result of the deformation in cohesive zone model being smaller and the fracture process zone being bigger.

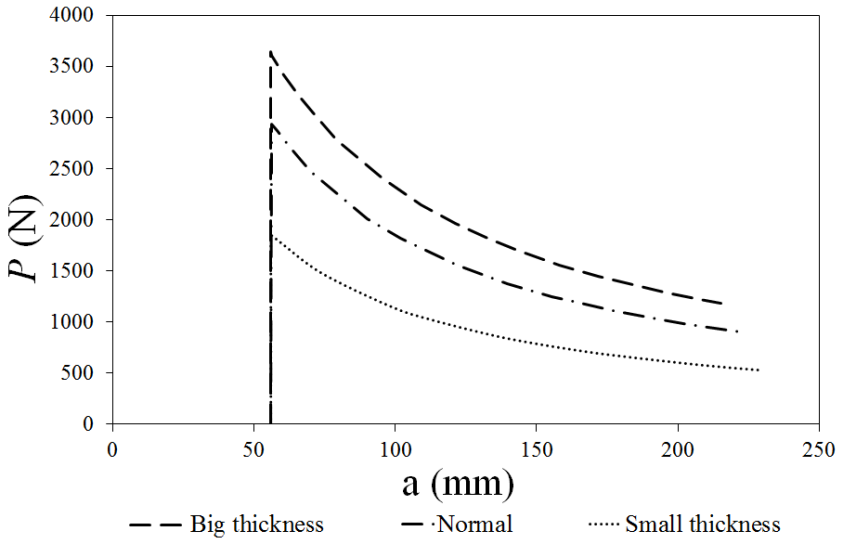

Figure 49 – Numerical *P-a* curve of three different substrates thicknesses.

a)

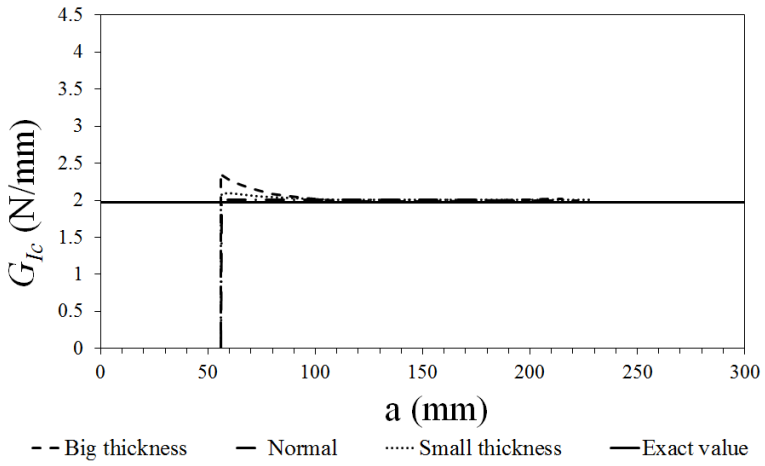

b)

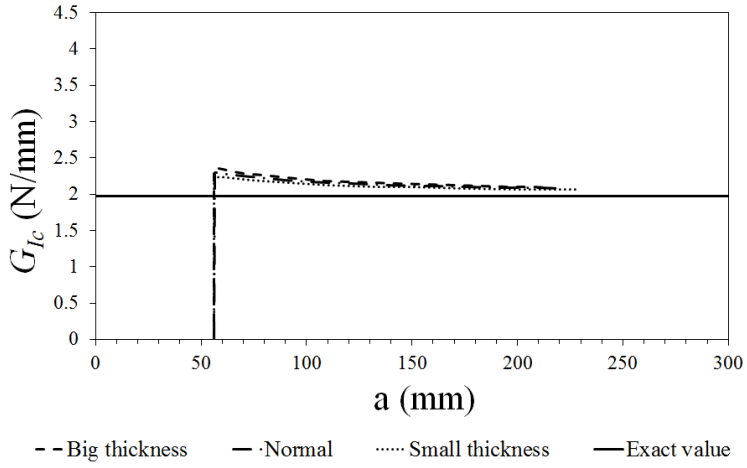

c)

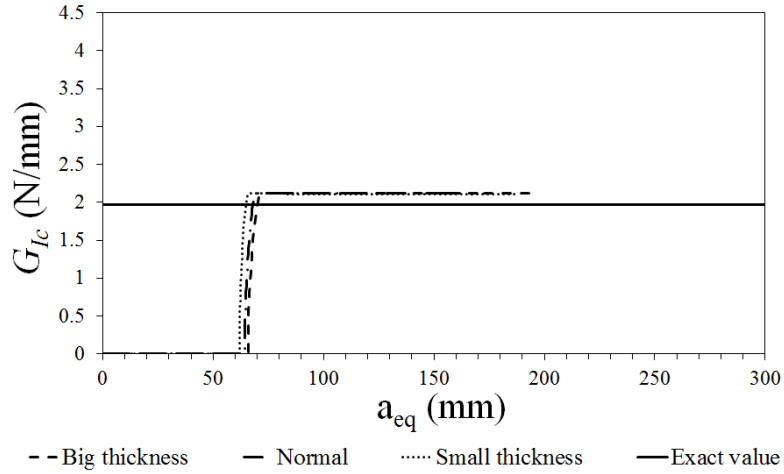

Figure 50 – Numerical R-cures of the three different substrate thicknesses using: a) CCM method, b) CBT method, c) CBBM method.

The CCM method has a deviation in the initial crack toughness opposed to the CBT. This is a result of the correction of the deformation around the crack tip introduced by the later. The CBBM method is also corrected and the initial fracture toughness is similar in all cases. However the a_{eq} presents a different initial crack length in all tests

because it accounts for the fracture process zone (FPZ). The stiffer the substrates the bigger the initial FPZ and the bigger is the initial crack length (equivalent).

There is a consistent decrease in toughness in the plateau region for the CBT method. For the other two methods used the values are similar.

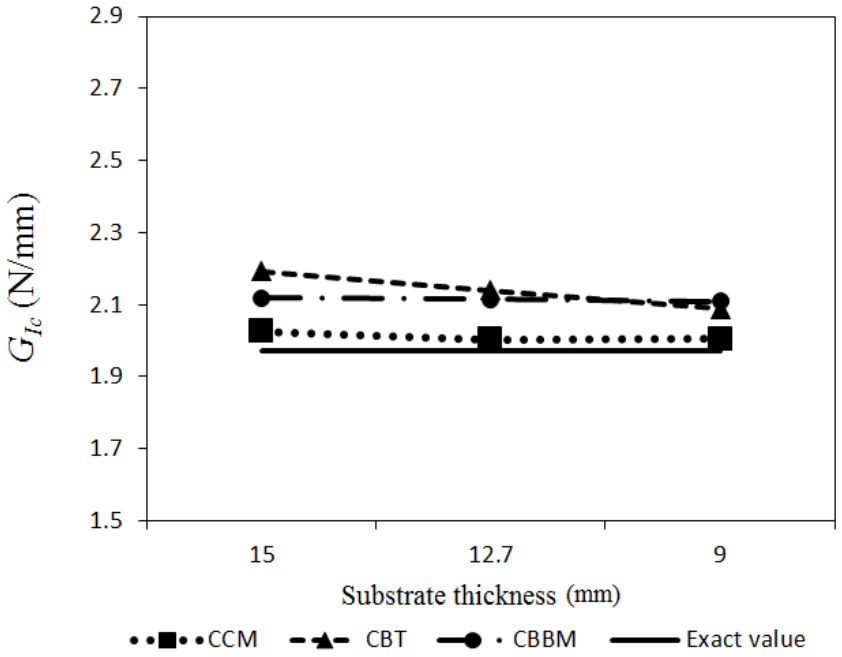

Figure 51 – Comparison of the numerical fracture toughness in the plateau region of the R-curve for three different substrate thicknesses and three different methods: CCM, CBT and CBBM

e) Different materials

Two normal DCB specimens with different materials, steel and aluminium, were tested. The linear elastic properties of aluminium were used for the substrates, Young´s modulus of 80 GPa and 0.33 for the Poisson´s ratio.

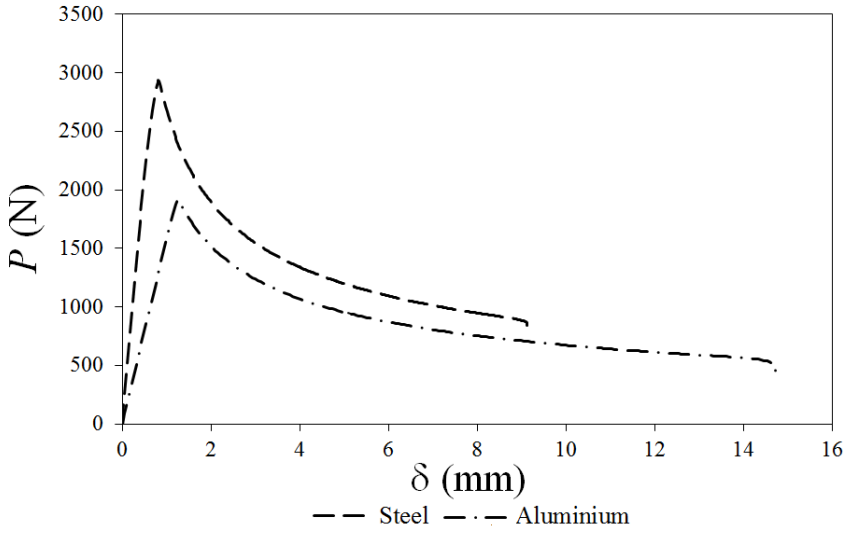

Figure 52 – P-δ curve of two DCB specimens with different materials for adherends.

The initial linear loading of the aluminium specimen is less rigid and the final displacement, in the loading line, is higher in accordance with its lower Young´s modulus. Also failure and crack propagation occurs at lower loads (Figure 52 and Figure 53) as a consequence of a smaller FPZ.

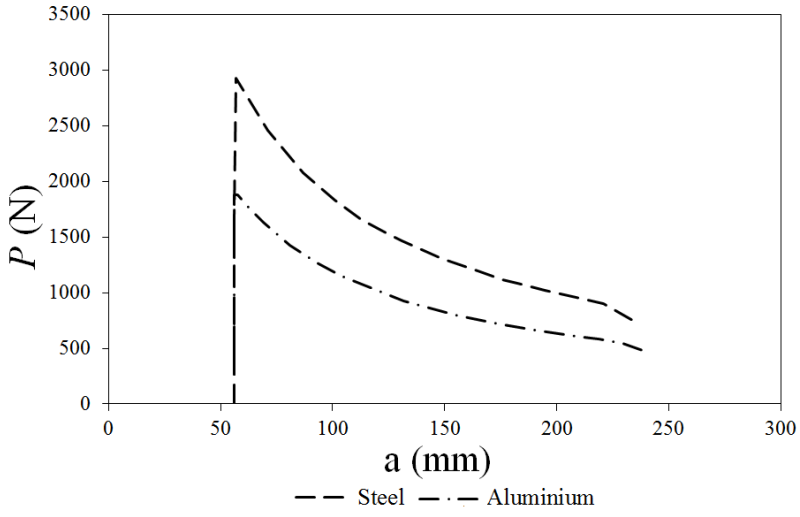

Figure 53 - P-a curve for the two different materials.

The stresses were analysed using the von Mises criteria to evaluate if a normal aluminium specimen would deform plastically.

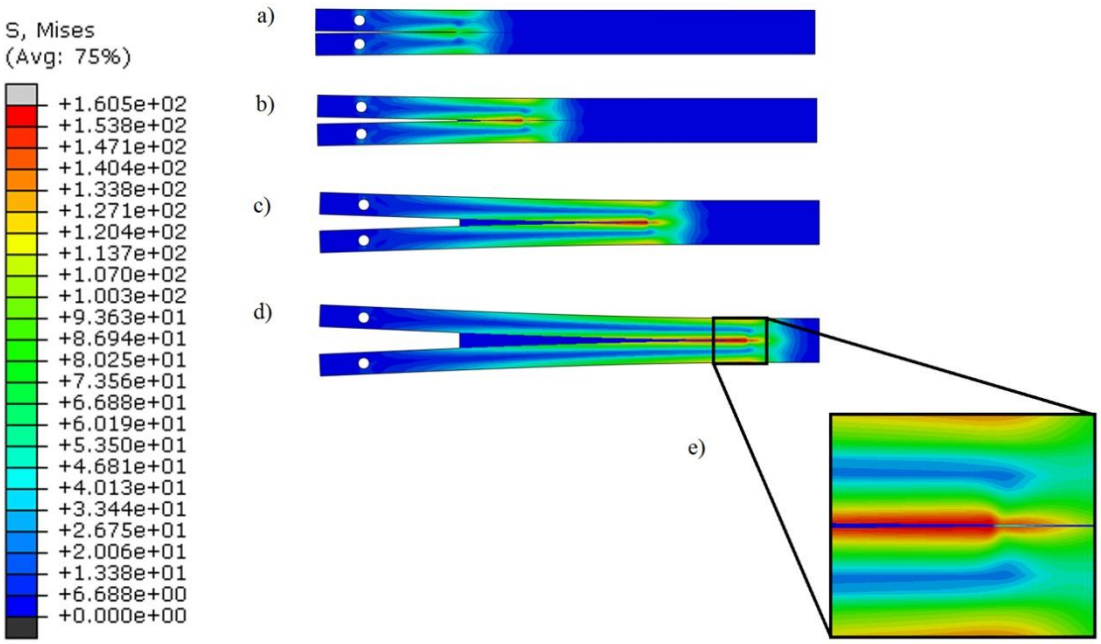

Figure 54 – von Mises stresses during the DCB test simulation, a) to d) frames of the test from the beginning to the end and e) an amplification of the critical part of the specimen.

The stress of 160 MPa in the adherends near the adhesive layer would cause deformation of a low strength aluminium substrate. Although some aluminium alloys and heat treatments can provide such strength it is easier to use hard steel for the small DCB prototype.

The shape of the R-curves, in Figure 55, for the CCM method is very similar with an almost perfect overlap.

a)

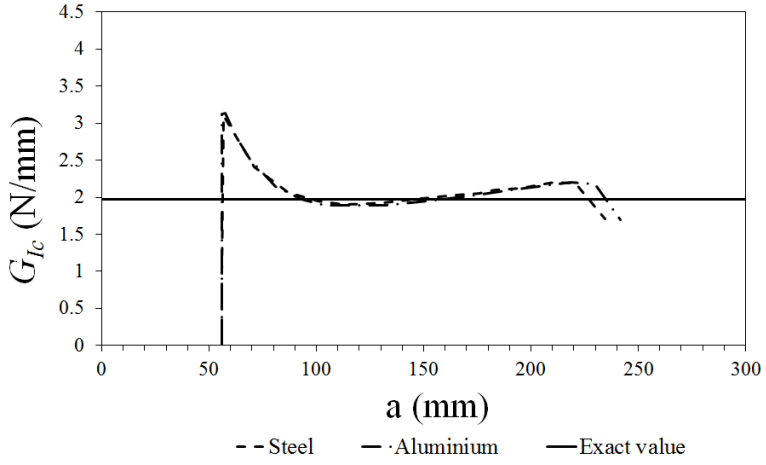

Figure 55 (continues) - Numerical R-curves of the two different materials, a) CCM method, b) CBT method, c) CBBM method.

b)

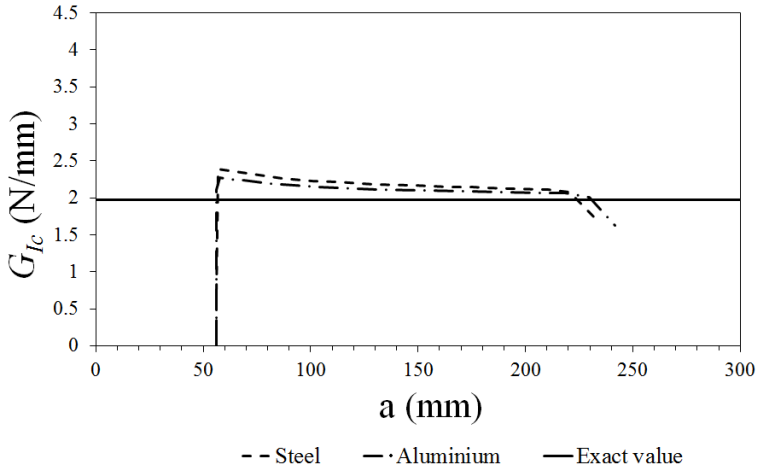

c)

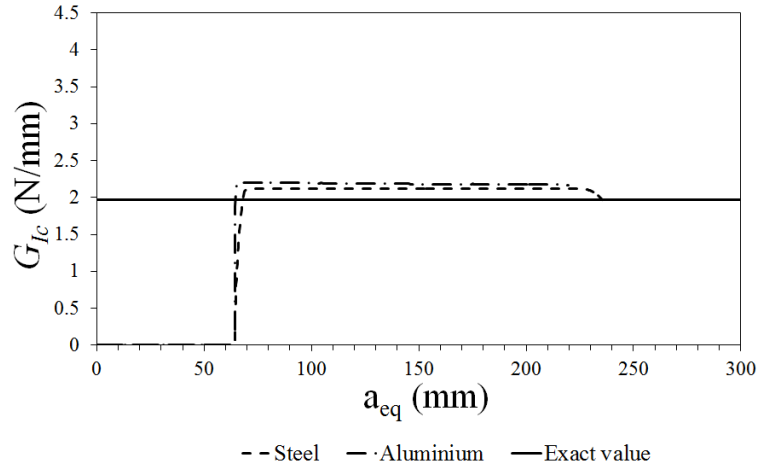

Figure 55 (continued)

Also in Figure 55 the CBT and CBBM have contradicting results. For the CBT the fracture toughness in the R-curve is always higher for the steel simulation and in contrast the CBBM gives opposite results. Experimental results have confirmed an increase in toughness for softer substrates but this phenomenon is not taken into account in the numerical simulation. [27]

Both fracture toughness in the plateau region were similar in the CCM method (Table 6). For the other two methods there is a higher deviation.

Table 6 – Compilation of the fracture toughness calculated using the CCM, CBT and CBBM.

	CCM	CBT	CBBM
Steel	2.04 ± 0.14	2.19 ± 0.06	2.11 ± 0.00
Aluminium	2.02 ± 0.10	2.12 ± 0.04	2.18 ± 0.01

f) Final specimen

After the evaluation of different parameters a final specimen was designed. The small specimen geometry is presented in Figure 56 and a similar finite element analysis as the previously presented was conducted.

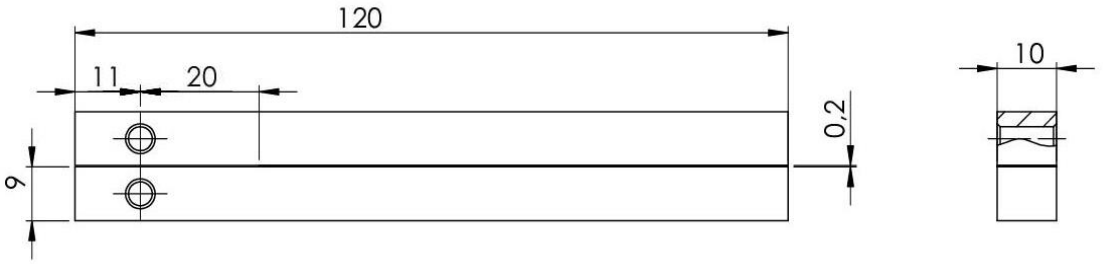

Figure 56 – Geometry of the small DCB specimen; final specimen (dimensions in mm)

Both *P-δ* curves shown below have a similar shape and although there is a smaller initial crack in the short specimen the force up to failure is reduced due to the smaller width.

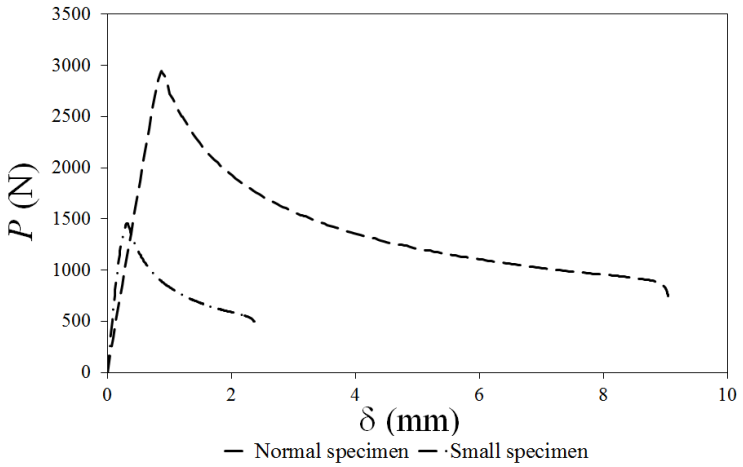

Figure 57 - Numerical P-δ of a normal and a small DCB specimen.

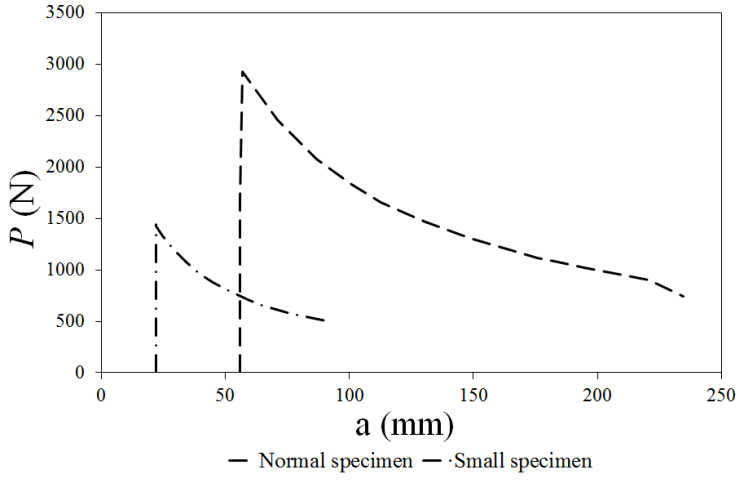

Figure 58 – P-a curve for the normal and a small DCB specimen.

From the three models used to calculate fracture toughness only the CBT and CBBM worked and gave reasonable R-curves (Figure 43).

a)

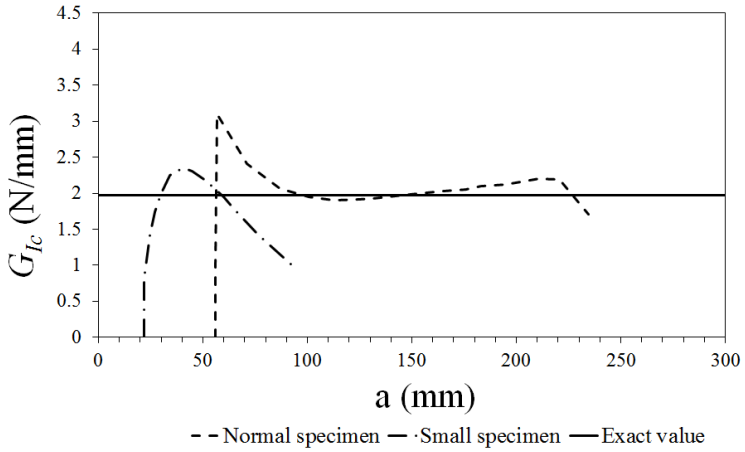

b)

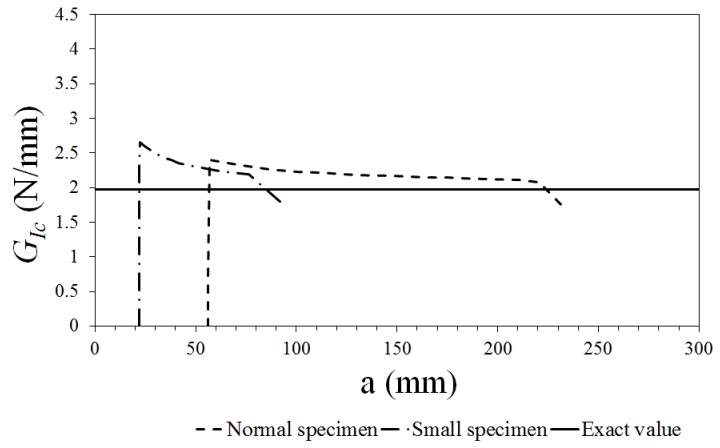

c)

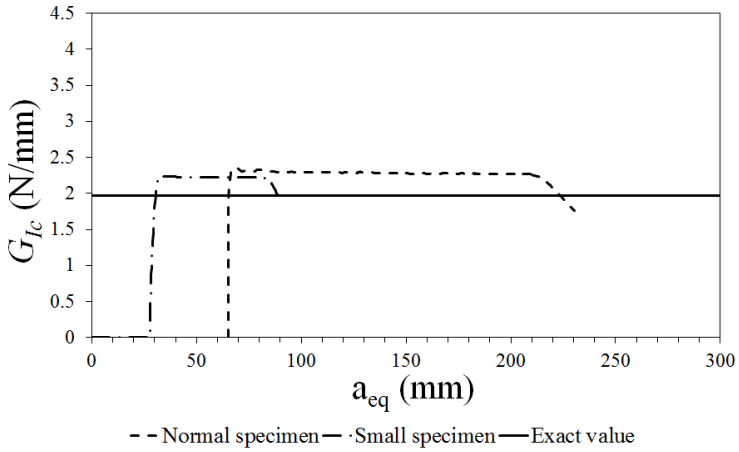

Figure 59 – Numerical R-curves for the normal and small DCB specimen, a) CCM method, b) CBT method, c) CBBM method.

The shape of the CCM method presented in Figure 59, a), does not have either a plateau or the shape that would be expected for stable damage propagation in the adhesive. In contrast, the two other methods accurately calculated the fracture toughness of the adhesive (Table 7).

Table 7 - Summary of the fracture toughness calculated using the CCM, CBT and CBBM.

	CCM			CBT			CBBM		
Normal DCB	2.04	±	0.14	2.19	±	0.06	2.28	±	0.01
Small DCB	-	±	-	2.33	±	0.07	2.23	±	0.00

The stresses in the specimen were studied. The tensions in the final specimen are equal to the normal DCB specimen and as a result the same steel can be used effectively. The distribution of tension in the final specimen is presented below.

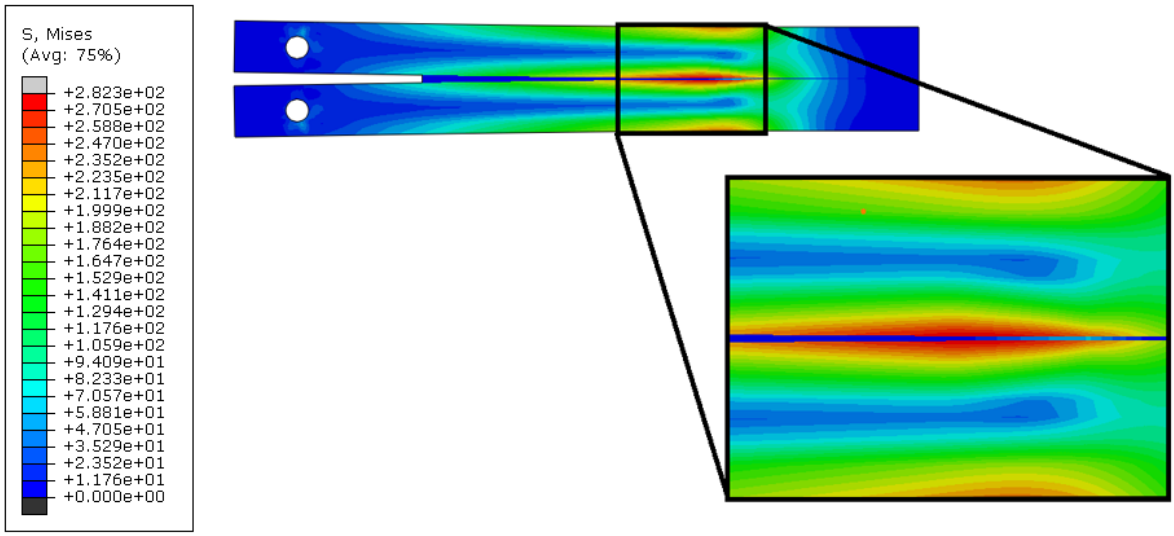

Figure 60 - von Mises stresses during the final DCB test simulation.

The final specimen has the required dimensions of less than 120 mm from the loading line to the wall and will fit in the chamber to be used in the subsequent durability project.

4.2 Experimental DCB tests

4.2.1 Experimental procedure

a) Adhesive

The epoxy adhesive SikaPower 4720 was used, supplied by SIKA® (Portugal, Vila Nova de Gaia). This adhesive is a two-part system that cures at room temperature for 24 hours. It has a tensile strength of 25 MPa and an elongation at break of 4%.

b) Substrates

In the DCB tests, a high tensile strength steel (DIN 40 CrMnMo 7) was used to avoid plastic deformation of the substrates. The general properties of the steels used are presented in Table 8.

Table 8 - Mechanical properties of the steel used for the substrates of the DCB specimens.

Standard	Young's modulus (GPa)	Yield Strength (MPa)	Tensile strength (MPa)	Strain (%)
DIN 40 CrMnMo 7	205	895.5± 34.5	1034± 34	15.5± 1.5

c) Specimen manufacture

The geometry of the normal and final DCB test specimens of the numerical study of this thesis were used and are given again in Figure 61 for convenience. In order to prepare the specimens, firstly the surface of the substrates was grit blasted and degreased with acetone prior to the application of adhesive. To guarantee the adhesive bondline thickness, spacers were inserted between the adherends on both ends. On one end, two steel plates and a razor blade of 0.1 mm was inserted to introduce a pre-crack and guarantee cohesive failure propagation from the beginning of the test. On the other end, one steel plate was inserted to guarantee a bondline thickness of 0.2mm. Adhesive was applied in both adherends before assembly and were set in a mold for correct alignment while curing (Figure 62). Lastly, the joints were left under 2 MPa pressure for 24h at room temperature in a hydraulic hot plates press. After curing the spacers were removed along with any excess adhesive. The bondline thickness was controlled using an optic microscope.

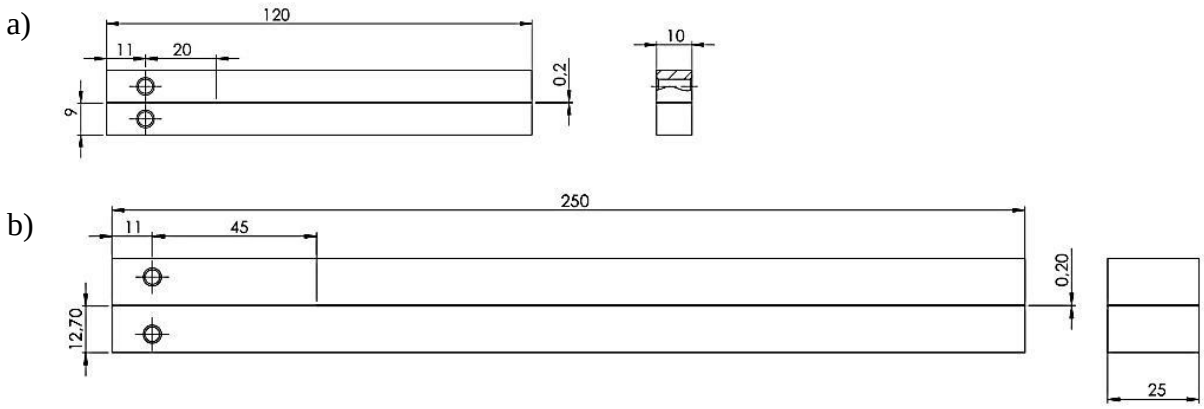

Figure 61 - Geometry of the DCB specimens tested, a) small specimen, b) normal specimen.

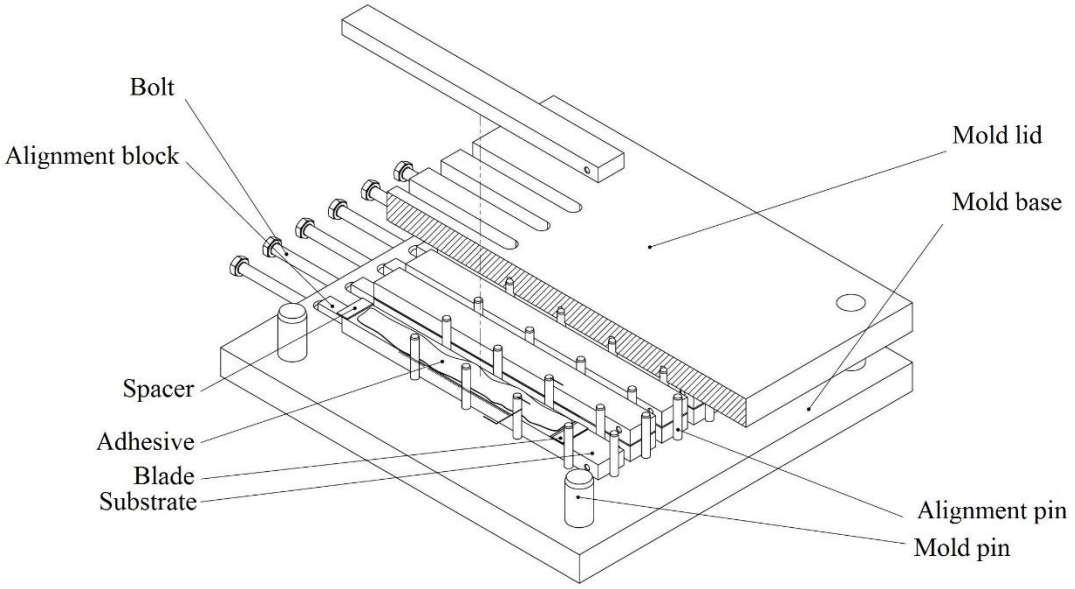

Figure 62 - Schematic representation of the mold used to cure the DCB specimens with the respective legend.

d) Test procedure

The specimen were tested according to standard ASTM D3433 in a INSTRON® model 3367 universal test machine (Norwood, Massachusetts, USA) with a capacity of 30 kN, at room temperature and constant displacement rate of 0.2, 0.5 and 2 mm/min. The specimen was loaded to measure the behaviour of the adhesive to fracture in mode I. Pictures were recorded during the testing with 5 s intervals using a 10 MPixel digital camera. These images allowed the measurement of the crack length during its growth. Loads and displacements were recorded up to failure. Four specimens were tested for each geometry.

4.2.2 Experimental results and discussion of DCB tests

a) Characterization of fracture toughness

Four normal DCB tests were conducted with a displacement rate of 0.5 mm/min to characterize the adhesive toughness in mode I. One typical *P-δ* curve obtained with this method is presented in Figure 63.

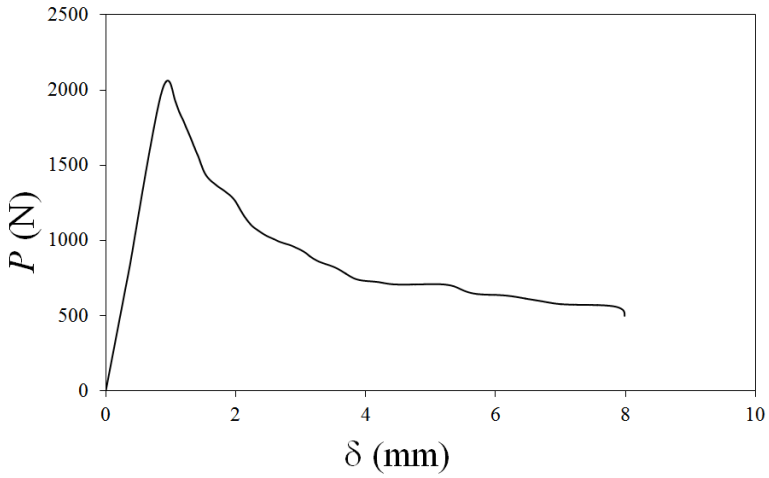

Figure 63 – Example of the P-δ obtained, specimen 4.

For each normal specimen an R-curve was calculated similar to the curve shown in Figure 64.

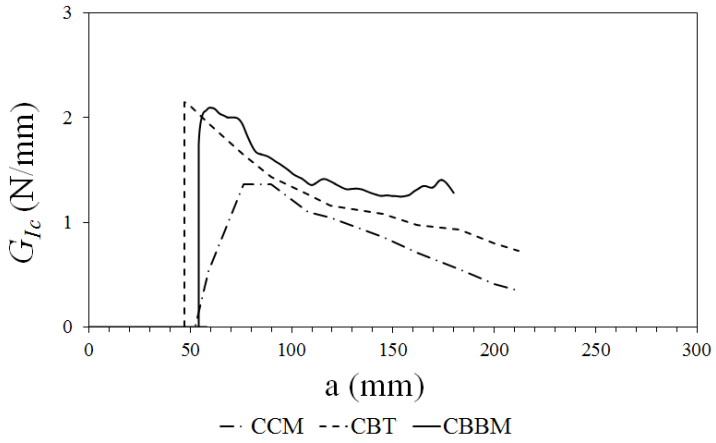

Figure 64 – Example of an R-curve obtained, specimen 4.

The final value of 1.53 N/mm (value determined using the average of the techniques showed in Table 9) is much higher than conventional toughened epoxy adhesives (0.3-0.6 N/mm) and comparable to that of a polyurethane adhesive (1.2-2.9 N/mm). [28]

Table 9 – Values of the fracture toughness of adhesive SikaPower 4720 using the normal specimen.

	CCM	CBT	CBBM
G_{IC} (N/mm)	1.38 ± 0.18	1.58 ± 0.15	1.63 ± 0.07

b) Displacement rate

Three displacement rates were compared, 0.2, 0.5 and 2 mm/min to study the effect of strain rate on the fracture toughness (Figure 65).

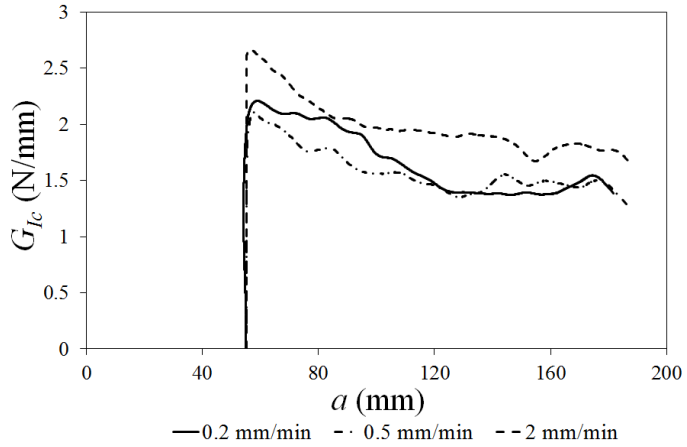

Figure 65 - Comparison of three R-curves using the CBBM method for different velocities.

For the two lowest displacement rates, 0.2 and 0.5 mm/min, the values of fracture toughness were almost the same (Figure 64). On the other hand the displacement rate of 2 mm/min had an increase in toughness which can be a result of the adhesive's viscoelastic behaviour.

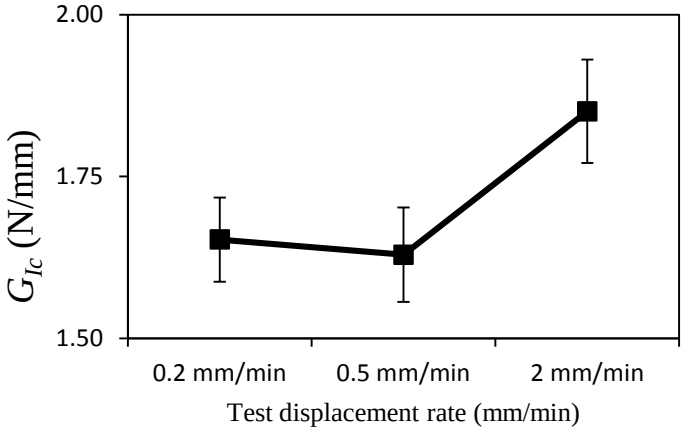

Figure 66 – Comparison of the fracture toughness of SikaPower 4720 with different displacement rates.

The rupture was cohesive in all tests and a picture of the facture surface is presented in Figure 67. As a note, the fracture surface of the DCB specimens with 2 mm/min displacement had less rugosity than the specimens tested with slower velocities and is further proof that viscoelastic behaviour has to be taken into account.

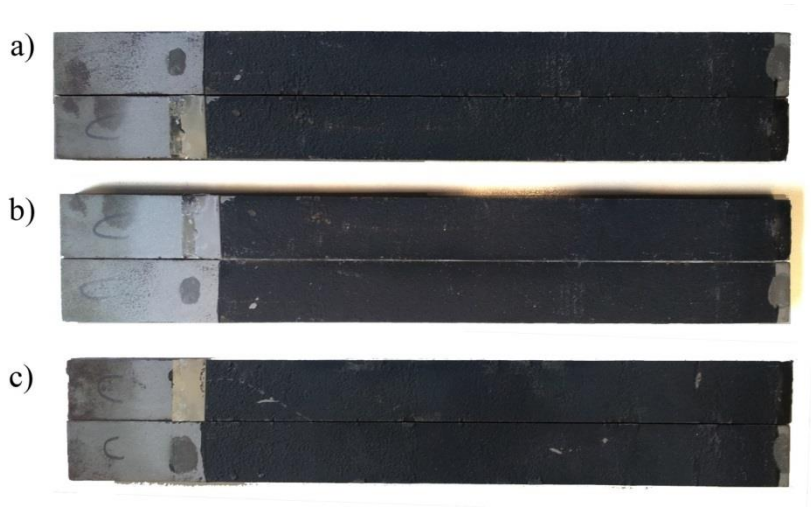

Figure 67 – Example of the failure mode of DCB specimens with SikaPower 4720 using three different displacement rates, a) 0.2mm/min, b) 0.5mm/min and c) 2 mm/min.

c) Comparison of two different DCB specimens

The initial rigidity of the specimens is not the same for all the cases (Figure 68). A part of the reason is the variation of the initial crack length for the normal and short DCB specimens. The normal specimens have a mean value of 46.35 mm (45 idealized) and a standard deviation of 0.68 for the initial crack length. There was a better result for the short specimen of 19.93 mm (20mm idealized) of crack length with a standard deviation of 0.18 mm.

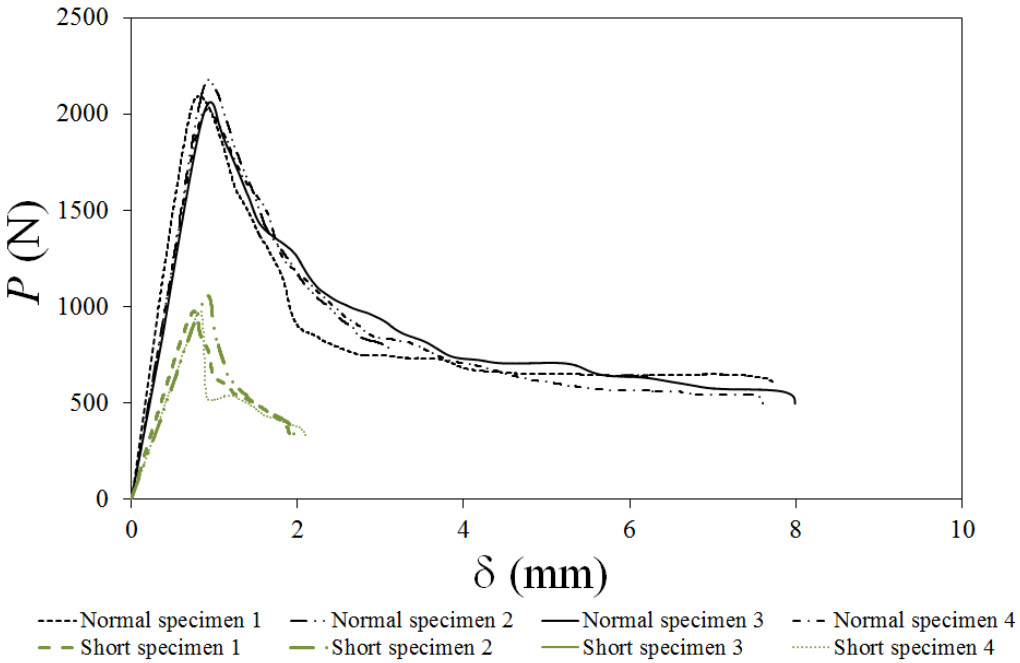

Figure 68 – *P-δ* curve for the short and normal DCB specimens tested with SIKA® 4720.

Throughout the work done with the normal and small specimens it is clearly much easier to control the manufacturing process for the small specimens, ex. bondline thickness and the initial crack length.

Only the CBBM method was used in the analysis of the small DCB specimens. The first reason was due to the better results in the numerical study and on top of it a technical difficulty. The initial crack of the small DCB specimen was obstructed by the machines holding mechanism making it impossible to monitor the beginning of the failure propagation.

The initial fracture toughness is very high for the small specimen (Figure 69). Since it was a toughened adhesive the initial crack introduced by the blade may not have been sufficient to introduce a high enough stress concentration factor. Also the concept of linear elastic fracture mechanics implies that plasticity should be limited to a small region ahead of the crack tip and a long enough crack should exist. Most likely neither verify in the testing of the small specimen.

There was a stable propagation in all small specimens. [11]

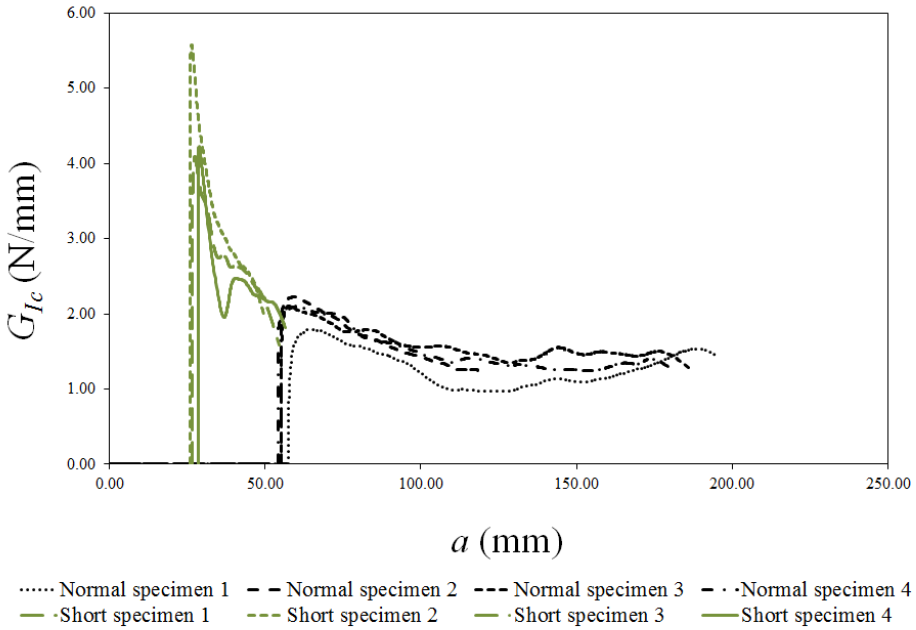

Figure 69 – R-curve of the small specimen and normal specimen using the CBBM method.

The rupture was cohesive in all tests and a picture of the facture surface is presented in Figure 70.

Figure 70 - Two examples of the cohesive fracture surface of the specimens tested, a) small specimen and b) normal specimen.

5. Impact tests

5.1 Experimental procedure

5.1.1 Adhesive

The epoxy adhesive XNR6852 was used, supplied by NAGASE CHEMTEX® (Osaka, Japan).

5.1.2 Substrates

A ductile steel (DIN St33), used in car body shells, was used in order to study the effect of adherend yielding on the joint strength. The properties of the steel can be found in Table 10.

Table 10 – Mechanical properties of the substrates in SLJ

Standard	Young's modulus (GPa)	Yield Strength (MPa)	Tensile strength (MPa)	Strain (%)
DIN St33	205	183.8	288	17.6

5.1.3 Specimen manufacture

The geometry for the SLJ test specimen is given in Figure 71. By attaching two steel plates at the end of the SLJ specimen with mild steel there is improved grip during the test. The joint surfaces were grit blasted and degreased with acetone prior to the application of adhesive. After the surface preparation an overlap of 50 mm was constructed. The thickness of the adhesive bond line was 0.2 mm. All the joints were manufactured without a fillet.

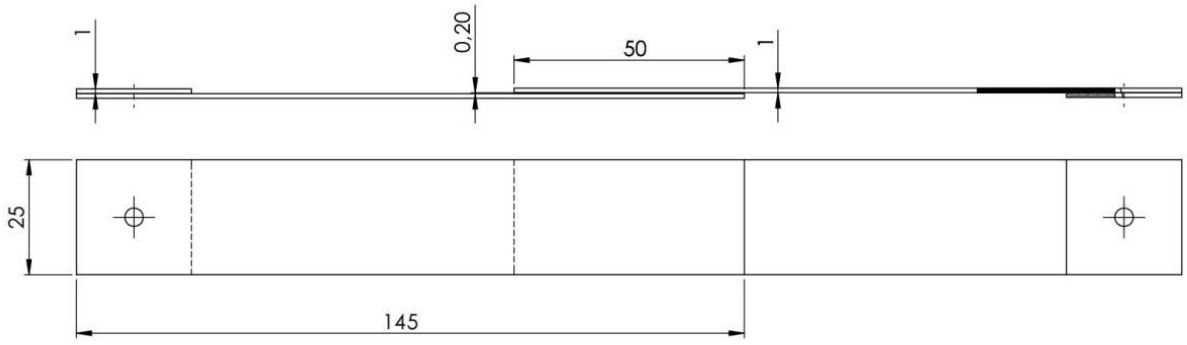

Figure 71 – Geometry of the SLJ used for the impact tests (dimensions in mm).

A mold with spacers for correct alignment of the substrates was used to produce the SLJ specimens (Figure 72). The substrates were bonded and the joints left under 2 MPa pressure for 3 h at 150 ºC in a hydraulic hot plates press, being removed from the mold along with any excess adhesive at the end of the curing process.

This geometry was chosen because it is usually used and will therefore enable comparison with other academic work. Furthermore it is representative of a structural part.

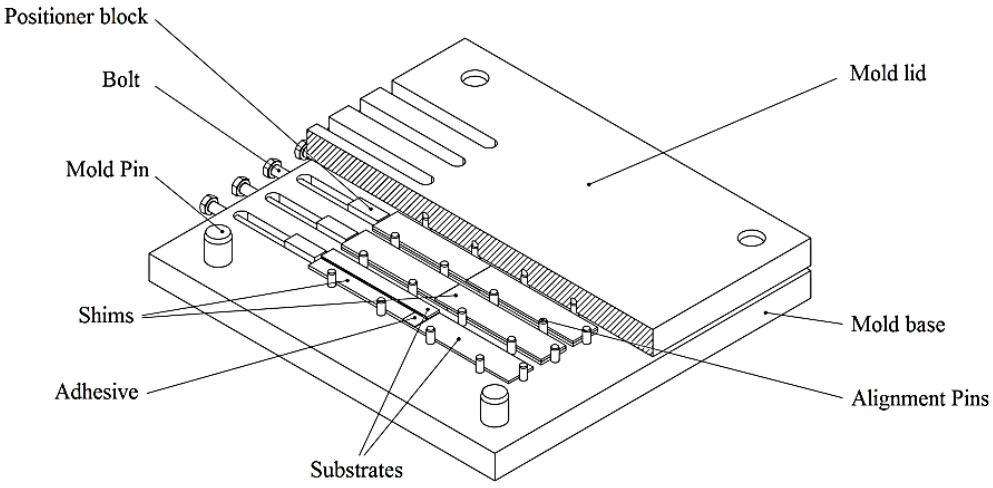

Figure 72 - Schematic mold for SLJ specimens.

5.1.4 Test procedure

The tests were conducted in Rosand® Intrumented Falling weight impact tester, type 5 H.V. (Stourbridge, West Midlands, U.K.). The machine was calibrated to give an energy at impact of 300 J loading the specimen in tension. The energy was dissipated in the specimen from a falling mass of 29.83 kg with a velocity approximately equal to 4.47 m/s.

5.2 Experimental results and discussion

Due to the high strain rate the steel adherends had a different behaviour when comparing with the quasi static test, deforming less and absorbing less energy (Table 11 and Figure 73). As a result of the strain rate dependence of the steel, the failure load was increased but the adhesive experienced a similar damage as in the case of static loading.

Table 11 - Energy (J) and failure load (N) values obtained from the quasi-static and impact test.

	Energy (J)	Failure load (kN)
Quasi-static test	291.64 ± 22.17	7.26 ± 0.04
Impact test	260.09 ± 7.69	12.22 ± 0.57

For application where impact energy absorption is important well-constructed adhesive joints with a high elongation epoxy such as the studied is interesting for it has a high damage tolerance, high elongation and high strength.

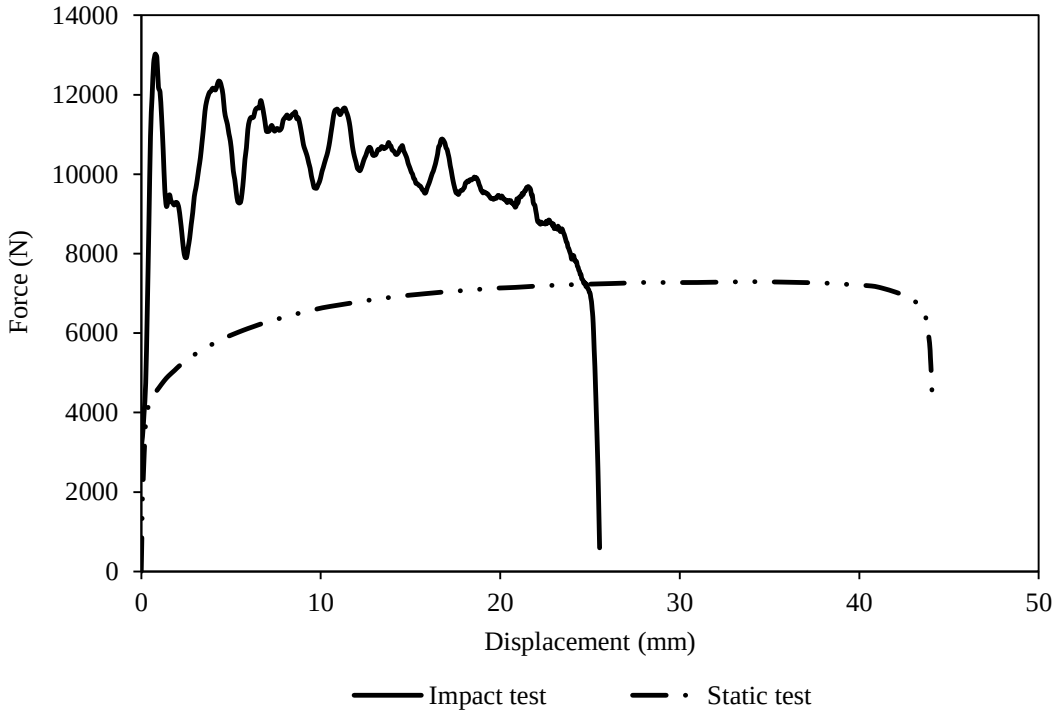

Figure 73 - Comparison of SLJ with mild steel adherends under two different strain rates.

The rupture was in all cases in the steel adherends (Figure 74). Under high strain rate the same failure mode as in the quasi-static tests was obtained and again a case of plane stress was observed in the steel adherend.

Figure 74 – Failure mode of the SLJ tested

6. Conclusions

A characterization of two adhesives was done. The adhesive XNR 6852 has:

- High tensile strength (approximately 60 MPa), typical of an epoxy adhesive.
- High elongation (approximately 100%), typical of a polyurethane adhesive.
- Can withstand deformation and damage without a brittle behavior for both impact and quasi-static cases.
- High toughness (G_{IC} = 1.97 N/mm and G_{IIC} = 12.5 ±1.1), typical of a polyurethane adhesive.

The adhesive SikaPower 4720 has:

- Low tensile strength (approximately 25 MPa) for an epoxy adhesive.
- Normal elongation and Young´s modulus (approximately 4% and 2000 MPa respectively) for an epoxy adhesive.
- High toughness (G_{IC} = 1,31 N/mm).

From the numerical study of fracture toughness in mode I using a DCB geometry it was concluded that:

- The smaller the crack length the higher the fracture toughness.
- Specimen length, width and substrate thickness do not have much influence on the fracture toughness

A small DCB specimen was put forward and:

- Numerical results suggested that a good and similar result for fracture toughness would be achieved using CBBM and CBT method but experimental results have proved otherwise for CBBM. A small DCB specimen increases the toughness because G_{IC} formulation is heavily dependent on the initial crack length and specimen compliance.

7. Future work

Study the small bulk specimens with other adhesives and compare with the results from the long dogbone.

Improve the results for the short DCB specimen studying other parameters.

Validate the numerical findings of the DCB simulations.

Using bulk specimens developed to study the water aging process of the both, NAGASE CHEMPTEX® XNR 6852 and SikaPower® 4720.

References

[1] da Silva L.F.M., Öchsner A., Adams R.D., Handbook of Adhesion Technology, 1 ed., Springer, Berlin, 2011.
[2] Kinloch A.J., Adhesion and Adhesives, Science and Technology., 1 ed., Chapman and Hall, Great Britain, 1987.
[3] Banea M.D., Da Silva L.F.M., Adhesively bonded joints in composite materials: An overview, Proceedings of the Institution of Mechanical Engineers, Part L: Journal of Materials: Design and Applications, 223 (2009) 1-18.
[4] Hartshorn S.R., Structural Adhesives, Chemistry and Technology., Hartshorn, 1986.
[5] Adams R.D., Wake W.C., Structural Adhesive Joints in Enginering, ELSEVIER APPLIED SCIENCE PUBLISHERS LTD, 1984.
[6] Adams R.D., Adhesive bonding, Science, technology and applications, Woodhead Publishing Limited, 2000.
[7] Lees W.A., Adhesives in Engineering Design, Springer-Verlag, The Design Council, 1984.
[8] da Silva L.F.M., das Neves P.J.C., Adams R.D., Spelt J.K., Analytical models of adhesively bonded joints—Part I: Literature survey, International Journal of Adhesion and Adhesives, 29 (2009) 319-30.
[9] da Silva L.F.M., das Neves P.J.C., Adams R.D., Wang A., Spelt J.K., Analytical models of adhesively bonded joints—Part II: Comparative study, International Journal of Adhesion and Adhesives, 29 (2009) 331-41.
[10] da Silva L.F.M., Öchsner A., Modeling of Adhesive Bonded Joints, Springer, 2008.
[11] Kanninen M.F., Popelar C.H., Advanced Fracture Mechanics, Oxford University Press, 1985.
[12] da Silva L.F.M., Dillard D.A., Blackman B.R.K., Adams R.D., Testing Adhesive Joints, Best practices., WILEI-VCH, 2012.
[13] Kanninen M.F., Popelar C.H., Advanced Fracture Mechanics, Oxford University Press.
[14] Robinson P., Das S., Mode I DCB testing of composite laminates reinforced with z-direction pins: a simple model for the investigation of data reduction strategies, Engineering Fracture Mechanics, 71 (2004) 345-64.
[15] de Moura M.F.S.F., Gonçalves J.P.M., Chousal J.A.G., Campilho R.D.S.G., "Cohesive and continuum mixed-mode damage models applied to the simulation of the mechanical behaviour of bonded joints, International Journal of Adhesion and Adhesives, 2008.
[16] de Moura M.F.S.F., Gonçalves J.P.M., Chousal J.A.G., Campilho R.D.S.G., Cohesive and continuum mixed-mode damage models applied to the simulation of the mechanical behaviour of bonded joints, International Journal of Adhesion and Adhesives, 28 (2008) 419-26.
[17] Banea M.D., Silva L.F.M.d., Campilho R.D.S.G., Effect of Temperature on Tensile Strength and Mode I Fracture Toughness of a High Temperature Epoxy Adhesive, Journal of Adhesion Science and Technology, 26 (2012) 939-53.
[18] Tsujimura T.Y., High toughness composites based on insitupolymerizable thermoplastic epoxy-resin, 29th International Conference and Forum -SAMPE Europe SEICO 08, Paris, 2008.
[19] Karachalios E.F., Adams R.D., da Silva L.F.M., Single lap joints loaded in tension with high strength steel adherends, International Journal of Adhesion and Adhesives, 43 (2013) 81-95.

[20] Gordon K., Quasi-static strength and fatigue life of hybrid (bonded/bolted) composite single-lap joints, Composite Structures, 72 (2006) 119-29.
[21] Banea M.D., da Silva L.F.M., Static and fatigue behaviour of room temperature vulcanising silicone adhesives for high temperature aerospace applications. Statisches Verhalten und Dauerfestigkeitsanalyse von vulkanisierten Silikonklebstoffen für Luftfahrtanwendungen bei hohen Temperaturen, Materialwissenschaft und Werkstofftechnik, 41 (2010) 325-35.
[22] Wang Y., Williams J.G., Corrections for mode II fracture toughness specimens of composites materials, Composites Science and Technology, 43 (1992) 251-6.
[23] Yoshihara H., Kawamura T., Mode I fracture toughness estimation of wood by DCB test, Composites Part A: Applied Science and Manufacturing, 37 (2006) 2105-13.
[24] de Moura M.F.S.F., Campilho R.D.S.G., Gonçalves J.P.M., Crack equivalent concept applied to the fracture characterization of bonded joints under pure mode I loading, Composites Science and Technology, 68 (2008) 2224-30.
[25] de Moura M.F.S.F., Campilho R.D.S.G., Gonçalves J.P.M., Crack equivalent concept applied to the fracture characterization of bonded joints under pure mode I loading, Composites Science and Technology, 2008.
[26] Banea M.D., L. F. M. Silva, and R. D. S. G. Campilho, Effect of temperature on tensile strength and mode I fracture toughness of a high temperature epoxy adhesive, Journal of adhesivion science and technology, 2011.
[27] Yan C., Mai Y.-W., Yuan Q., Ye L., Sun J., Effects of substrate materials on fracture toughness measurement in adhesive joints, International Journal of Mechanical Sciences, 43 (2001) 2091-102.
[28] da Silva L.F.M., Carbas R.J.C., Critchlow G.W., Figueiredo M.A.V., Brown K., Effect of material, geometry, surface treatment and environment on the shear strength of single lap joints, International Journal of Adhesion and Adhesives, 29 (2009) 621-32.

Appended papers